HCO_3^- Secretion by Murine Nasal Submucosal Gland Serous Acinar Cells during Ca^{2+}-stimulated Fluid Secretion

Robert J. Lee,[1] Janice M. Harlow,[1] Maria P. Limberis,[3] James M. Wilson,[3] and J. Kevin Foskett[1,2]

[1]Department of Physiology, [2]Department of Cell and Developmental Biology, and [3]Department of Pathology and Laboratory Medicine, Division of Medical Genetics, University of Pennsylvania, Philadelphia, PA 19104

Airway submucosal glands contribute to airway surface liquid (ASL) composition and volume, both important for lung mucociliary clearance. Serous acini generate most of the fluid secreted by glands, but the molecular mechanisms remain poorly characterized. We previously described cholinergic-regulated fluid secretion driven by Ca^{2+}-activated Cl^- secretion in primary murine serous acinar cells revealed by simultaneous differential interference contrast (DIC) and fluorescence microscopy. Here, we evaluated whether Ca^{2+}-activated Cl^- secretion was accompanied by secretion of HCO_3^-, possibly a critical ASL component, by simultaneous measurements of intracellular pH (pH_i) and cell volume. Resting pH_i was 7.17 ± 0.01 in physiological medium (5% CO_2–25 mM HCO_3^-). During carbachol (CCh) stimulation, pH_i fell transiently by 0.08 ± 0.01 U concomitantly with a fall in Cl^- content revealed by cell shrinkage, reflecting Cl^- secretion. A subsequent alkalinization elevated pH_i to above resting levels until agonist removal, whereupon it returned to prestimulation values. In nominally CO_2–HCO_3^--free media, the CCh-induced acidification was reduced, whereas the alkalinization remained intact. Elimination of driving forces for conductive HCO_3^- efflux by ion substitution or exposure to the Cl^- channel inhibitor niflumic acid (100 µM) strongly inhibited agonist-induced acidification by >80% and >70%, respectively. The Na^+/H^+ exchanger (NHE) inhibitor dimethylamiloride (DMA) increased the magnitude (greater than twofold) and duration of the CCh-induced acidification. Gene expression profiling suggested that serous cells express NHE isoforms 1–4 and 6–9, but pharmacological sensitivities demonstrated that alkalinization observed during both CCh stimulation and pH_i recovery from agonist-induced acidification was primarily due to NHE1, localized to the basolateral membrane. These results suggest that serous acinar cells secrete HCO_3^- during Ca^{2+}-evoked fluid secretion by a mechanism that involves the apical membrane secretory Cl^- channel, with HCO_3^- secretion sustained by activation of NHE1 in the basolateral membrane. In addition, other Na^+-dependent pH_i regulatory mechanisms exist, as evidenced by stronger inhibition of alkalinization in Na^+-free media.

INTRODUCTION

The secretion of airway surface liquid (ASL) and the control of its volume and composition are critical for the maintenance of mucociliary clearance and the ability to rid the lung of inspired pathogens and irritants (for review see Wine and Joo, 2004). In cartilaginous airways, submucosal exocrine glands secrete a large percentage of the NaCl-rich fluid and mucus that comprise the ASL (for review see Ballard and Inglis, 2004; Ballard and Spadafora, 2007), and a knowledge of both the regulation and composition of submucosal gland secretion is essential for understanding lung fluid homeostasis. Previous experimental studies of intact tissue preparations have provided insights into secretagogue-mediated regulation of these glands, including the rates of secretion and the volumes of the end-product secretions (Yang et al., 1988; Inglis et al., 1997a,b, 1998; Jayaraman et al., 2001; Joo et al., 2001a,b, 2002a,b, 2006; Song and Verkman, 2001; Salinas et al., 2005; Song et al., 2006; Wu et al., 2006; Ianowski et al., 2007). However, the complex structure and relative inaccessibility of airway submucosal glands have limited experimental studies of the ionic composition of the primary secretions and the molecular mechanisms by which the various cell types (serous, mucous, and both ciliated and nonciliated collecting duct cells) secrete and/or modify the fluid/mucous product.

Of particular interest are serous acinar cells present at the distal ends of submucosal glands, because they likely secrete the bulk of glandular fluid in response to secretagogues that use cAMP and/or Ca^{2+} as second messengers (Wu et al., 2006). The fluid secreted by serous acinar cells contributes directly to ASL volume and is also likely

Abbreviations used in this paper: AE, $Cl-/HCO_3-$ (anion) exchanger; AM, acetoxymethyl; ASL, airway surface liquid; BCECF, 2',7'-bis-(2-carboxyethyl)-5-(and-6)-carboxyfluorescein; CCh, carbachol; CF, cystic fibrosis; CFTR, cystic fibrosis transmembrane conductance regulator; DAPI, 4',6 diamidio-2-phenylindole; DIC, differential interference contrast; DMA, 5-(*N*,*N*-dimethyl)amiloride; DPBS, Dulbecco's PBS; EIPA, 5-(*N*-ethyl-*N*-isopropyl)amiloride; NBC, Na^+-HCO_3^- cotransporter; NFA, niflumic acid; NHE, Na^+/H^+ exchanger; NKCC1, Na^+ K^+ $2Cl^-$ cotransporter isoform 1; pH_i, intracellular pH; SNARF, seminaphtharhodafluor-5F 5-(and-6)-carboxylic acid; Wt, wild-type.

Correspondence to J. Kevin Foskett: foskett@mail.med.upenn.edu

The Rockefeller University Press $30.00
J. Gen. Physiol. Vol. 132 No. 1 161–183
www.jgp.org/cgi/doi/10.1085/jgp.200810017

crucial for proper hydration of mucin granules released from more proximal mucous cells (for review see Ballard and Inglis, 2004). Serous cells also play an important role in innate airway immunity by secreting lysozyme, lactoferrin (Raphael et al., 1989), various antimicrobial peptides such as defensins, and mucin macromolecules such as Muc7 (for reviews see Ballard and Inglis, 2004; Wine and Joo, 2004). Submucosal gland serous cells have been hypothesized to play a particularly critical role in the pathology of the disease cystic fibrosis (CF). CF is a disease caused by mutations in the cystic fibrosis transmembrane conductance regulator (CFTR), an apical membrane anion channel expressed in various epithelia, including the airway. In addition to conducting Cl^- and HCO_3^- (Poulsen et al., 1994), CFTR also may directly or indirectly regulate the activities of other ion channels and transporters, including the epithelial Na^+ channel (for review see Huang et al., 2004) and Cl^-/HCO_3^- exchangers (Lee et al., 1999a,b; Park et al., 2002; Ko et al., 2004). Immunochemical localization studies suggest that serous acinar cells are major sites of CFTR expression in the lung (Engelhardt et al., 1992; Jacquot et al., 1993). It has therefore been hypothesized that defects in the volume and/or composition of submucosal gland secretions caused by lack of CFTR contribute to the ASL dehydration that leads to impaired mucociliary clearance and the ultimately fatal lung damage from the resultant chronic bacterial infection that is a hallmark of CF pathology.

Because of the critical role of serous acinar cells in airway fluid physiology, we previously examined the ion transport mechanisms that underlie Ca^{2+} agonist–evoked fluid secretion in primary serous cells isolated from mouse nasal turbinate and septum (Lee et al., 2007). Agonists such as acetylcholine that elevate intracellular $[Ca^{2+}]$ ($[Ca^{2+}]_i$) are believed to be the major submucosal gland secretagogues in terms of the magnitude and rate of the fluid secretion response (Yang et al., 1988; Inglis et al., 1997b; Trout et al., 1998a; Joo et al., 2001b, 2002a,b; Wu et al., 2006). We combined differential interference contrast (DIC) microscopy with simultaneous quantitative fluorescence imaging of indicator dyes to measure the concentrations of ions involved in driving fluid secretion (Cl^-) and regulating it (Ca^{2+}). Cholinergic agonist-induced fluid secretion was shown to be reflected in cell volume changes that were indicative of changes in cell solute content underlying fluid secretion, suggesting that murine serous acinar cells secrete Cl^- and fluid in response to a rise in $[Ca^{2+}]_i$. The observed Ca^{2+}-evoked Cl^- secretion occurs through a Cl^- efflux pathway that is independent of CFTR, in agreement with observations of intact gland preparations from CF human lungs and CFTR-knockout (*cftr*$^{tm1Unc-/-}$) mice that suggested that cholinergic-stimulated fluid secretion remains intact in the absence of CFTR function (Jayaraman et al., 2001; Joo et al., 2002a; Thiagarajah et al., 2004; Salinas et al., 2005; Song et al., 2006; Ianowski et al., 2007).

In addition to their role in Cl^- secretion, we hypothesized that airway submucosal gland serous cells are likely important for secretion of HCO_3^- into the airway. Other exocrine gland acinar cells stimulated with cholinergic agonists exhibit marked decreases in intracellular pH (pH_i) that have been proposed to reflect loss of cellular HCO_3^- indicative of HCO_3^- secretion (Robertson and Foskett, 1994; Evans et al., 1999; Nguyen et al., 2000; Brown et al., 2003; Nguyen et al., 2004). To determine whether Ca^{2+}-mobilizing agonists stimulate HCO_3^- secretion from airway gland serous acinar cells, the DIC fluorescence microscopy technique was modified to simultaneously monitor agonist-induced cell volume changes (reflecting Cl^- secretion) and the fluorescence of seminaphtharhodafluor-5F 5-(and-6)-carboxylic acid (SNARF-5F), a quantitative ratiometric indicator of pH_i (reflecting changes in $[HCO_3^-]_i$), in combination with appropriate ion substitutions and pharmacology. The results outlined below suggest that cholinergic/Ca^{2+} stimulation of serous acinar cells leads to cytoplasmic acidification that results from a net efflux of cellular HCO_3^- via a niflumic acid (NFA)–sensitive pathway shared with Cl^-. Carbachol (CCh)-induced acidification is compensated for by up-regulation of the activity of the Na^+/H^+ exchanger isoform 1 (NHE1), which drives HCO_3^- secretion by raising pH_i and promoting conversion of intracellular CO_2 to HCO_3^-. These data contribute to the understanding of submucosal gland fluid secretion, the composition of serous cell secretions, HCO_3^- secretion mechanisms in the airway, and the mechanisms of pH_i regulation in serous cells.

MATERIALS AND METHODS

Reagents

Molecular biology reagents were obtained from Invitrogen. A rabbit polyclonal antibody against the 22–amino acid C terminus of rat NHE1 (100% homologous to the mouse NHE1 C terminus) and control antigenic blocking peptide were purchased from Alpha Diagnostic International. Polyclonal antiserum against the Na^+ K^+ $2Cl^-$ cotransporter isoform 1 (NKCC1) was a gift from R. James Turner (National Institute of Dental and Craniofacial Research, Bethesda, MD). Anti-CFTR monoclonal antibody 24-1 was purchased from R&D Systems, Inc. All microscope filters were obtained from Chroma Technologies, Inc. Cariporide (HOE 642; (4-isopropyl-3-methylsulfonyl-benzoyl)-guanidine methanesulfonate) and S3226 (3-[2-(3-guanidino-2-methyl-3-oxo-propenyl)-5-methylphenyl]-*N*-isopropylidene-2-methyl-acrylamide dihydrochloride) were gifts from Sanofi-Aventis Deutschland GmbH. All other reagents were purchased from Sigma-Aldrich unless otherwise noted.

Experimental Solutions

All experimental solutions were made fresh daily, with compositions listed in Table I. A vapor pressure osmometer was used to ensure that the osmolality was ~300 mOsm kg^{-1}. Unless noted, experiments were performed in one of two physiological salt solutions, Solution A (CO_2–HCO_3^--buffered; gassed with 95% O_2–5% CO_2)

TABLE I

Experimental Solution Compositions

Solution	A	B	C	D	E	F	G
NaCl	125[a]	125				5	41
NMDG-Cl			125	125	120–140		
KCl	5	5	5	5	5	60	57
K-Gluconate						80	32
$MgCl_2$	1.2	1.2	1.2	1.2	1.2		1.2
$MgSO_4$						0.8	
$CaCl_2$	1.2	1.2	1.2	1.2	1.2		1
Ca-Gluconate						1.6	
NaH_2PO_4	1.2	1.2					1.2
KH_2PO_4			1.2	1.2	1.2		
Glucose	11	11	11	11	11		11
Sucrose		10		10			
HEPES		10		10	10	20	
$NaHCO_3$	25						25
NMDG-HCO_3			25				
NH_4Cl					0, 5, 10, or 20		
pH_o	7.4	7.4	7.4	7.4	7.4	6.8, 7.2, or 7.6	7.4
gassed w/	5% CO_2/95% O_2	100% O_2	5% CO_2/95% O_2	100% O_2	100% O_2	100% O_2	5% CO_2/95% O_2

[a]All values for dissolved solids are mM.

or Solution B (HEPES-buffered, nominally CO_2–HCO_3^--free; gassed with 100% O_2). Experiments performed under Na^+-free conditions (with Na^+ isosmotically replaced by $NMDG^+$) were performed in Solution C. Experiments performed under both Na^+- and HCO_3^--free conditions were performed in Solution D. Intracellular pH_i buffering capacity was measured using Solution E (containing no Na^+ or HCO_3^- to neutralize all mechanisms of cellular pH_i regulation) with $[NH_3]_o$ = 0.6, 1.2, or 2.5 mM (at pH 7.4; made via isosmotic replacement of NMDG-Cl with 5, 10, or 20 mM NH_4Cl, respectively). Intracellular in vivo SNARF calibration was performed using high $[K^+]_o$ Solution F containing 10 µg/ml nigericin and pH_o values of 6.8, 7.2, and 7.6. Solution G (high $[K^+]_o$, low $[Cl^-]_o$) was used to experimentally block HCO_3^- efflux, as described in the text. In all experiments involving agonist stimulation, 100 µM CCh was used, previously shown to be a saturating concentration for both serous cells (Lee et al., 2007) and intact murine submucosal glands (Ianowski et al., 2007).

Under conditions of CO_2–HCO_3^- buffering, the pH_o and dissolved $[CO_2]_o$ of the extracellular medium are critical, because calculation of CO_2–HCO_3^--dependent intracellular buffering capacity (β_{HCO3-}) strongly depends on $[CO_2]_o$ (as described below), and because H^+ and HCO_3^- transport mechanisms are likely highly sensitive to $[H^+]$ and $[HCO_3^-]$ gradients. Because of the high CO_2 permeability of plastics, the CO_2–HCO_3^--buffered solutions were gassed in glass water-heated reservoirs connected with glass tubing to glass water-heated coils, where the solution was warmed before perfusion into the chamber containing the cells. Because a loss of dissolved $[CO_2]_o$ would be reflected in a rise in pH_o, solutions of 2',7'-bis-(2-carboxyethyl)-5-(and-6)-carboxyfluorescein (BCECF) free acid were used to confirm that pH_o = ~7.4 for gassed Solution A in the perfusion system (as shown in Fig. 1, A and B, and described in the legend). The temperature of the perfusate inside the perfusion chamber was measured daily using a digital thermometer (VWR Scientific) and probe (YSI, Inc.) and adjusted to ~37°C.

Murine Nasal Serous Acinar Cell Isolation

Murine serous acinar cells were isolated as previously described (Lee et al., 2007) from adult wild-type (Wt) or *cftr*$^{tm1Unc-/-}$ mice on a C57BL/6 background housed in a pathogen-free facility. Ages of the mice ranged from 3 to 7 mo. All procedures involving animals were handled according to regulations set out by the Institutional Animal Care and Use Committee of the University of Pennsylvania. In brief, nasal turbinate and septum were removed from mice killed via CO_2 asphyxiation followed by cervical dislocation. Tissue was immediately placed in ice-cold Solution B, minced finely with scissors, and then digested for ~45 min at room temp in $CaCl_2$-free Solution B supplemented with 1× MEM vitamins, 1× MEM amino acids, 2 mM L-glutamine, 1.5 mg ml^{-1} type IV collagenase (Worthington Biochemical Corp.), 0.28 U ml^{-1} liberase enzyme blend 3 (Roche Diagnostics Corp.), 10 µg/ml DNase I, and 0.8% BSA with gentle shaking and continuous gassing of 100% O_2. Cells were then washed via gentle centrifugation and resuspended in either Solution A or B (with continuous gassing as appropriate) supplemented with 1× "Complete" protease inhibitor cocktail (Roche Diagnostics Corp.). Serous cells were optically identified by size and visible morphology under DIC optics as previously described (Lee et al., 2007).

Simultaneous DIC Measurement of Cell Volume and Quantitative Fluorescence Measurements of pH_i and $[Ca^{2+}]_i$

Preliminary experiments were conducted with the pH-sensitive fluorescein derivative BCECF (Molecular Probes). However, observations suggested significant cellular toxicity as a result of BCECF illumination, including abnormally high resting pH_i (>7.6–7.8), rapid cytoplasmic acidification during the course of dye illumination (pH_i < 7.2 after ~2–3 min of typical fluorescence sampling), and failure to observe cell shrinkage in response to CCh (as previously reported by Lee et al., 2007). Therefore, pH_i measurements were instead made with SNARF-5F (Molecular Probes; Buckler and Vaughan-Jones, 1990; Liu et al., 2001). After plating on coverslips coated with Cell-Tak (BD Biosciences), isolated cells/acini were loaded with SNARF-5F by incubation in the acetoxymethyl (AM) ester derivative SNARF-5F-AM at a concentration of 5–10 µM for 10–15 min at room temperature in either Solution A or B with continuous gassing of 95% O_2–5% CO_2 or 100% O_2 as appropriate. After loading, the cells adhering to the coverslip were washed via gentle pipetting of Solution A or B

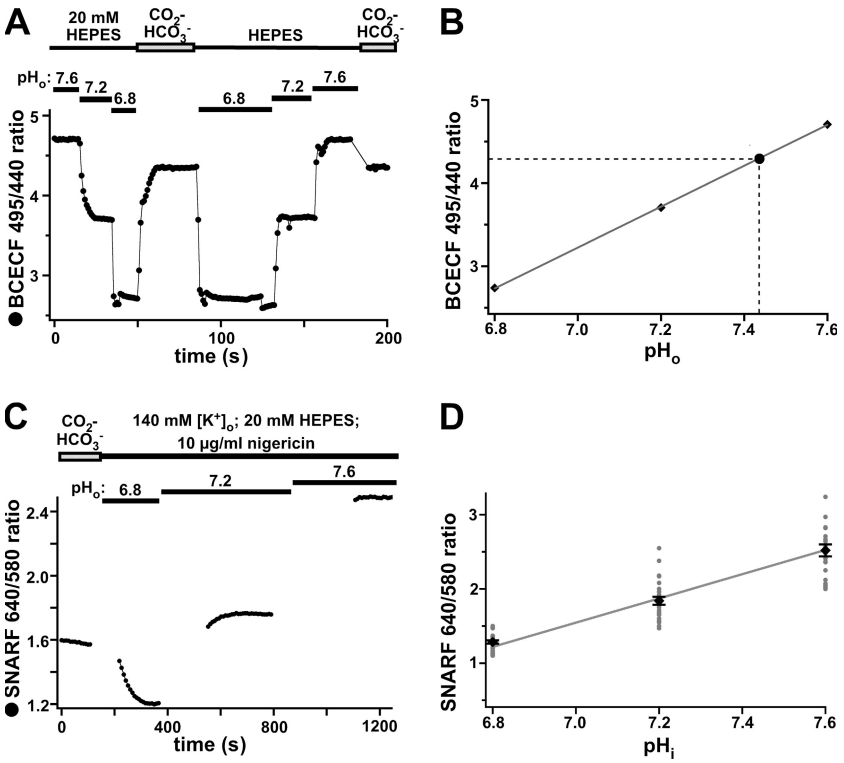

Figure 1. Measurement of extracellular CO_2–HCO_3^- buffer pH_o and in vivo calibration SNARF pH_i indicator fluorescence. (A) Measurement of pH_o under experimental conditions. The experimental perfusion system was loaded with either Solution A (5% CO_2–25 mM HCO_3^-) or Solution B (HEPES with pH_o = 6.8, 7.2, or 7.6 and ungassed) containing 0.5 µg/ml BCECF free acid. BCECF 495/440 nm fluorescence excitation ratios (emission collected at 535 nm) were measured upon switching between the solutions with different pH_o. (B) Mean BCECF fluorescence ratios (from experiment shown in A) were plotted vs. pH_o (diamonds). Mean ratios were 2.74, 3.71, and 4.71 for solutions of pH_o 6.8, 7.2, and 7.6, respectively. Solid line represents linear fit to the data with slope 2.46 ± 0.02 (s.d.) and intercept −14.0 ± 0.2 (s.d.). The BCECF fluorescence ratio in CO_2–HCO_3^--buffered Solution A (large black circle) was 4.32, corresponding to pH_o of ∼7.44. (C) Example of an in vivo SNARF fluorescence calibration experiment. A SNARF-loaded serous acinar cell was treated with 10 µg/ml nigericin and exposed to 140 mM $[K^+]_o$ solutions with pH_o = 6.8, 7.2, and 7.6. (D) Composite calibration of SNARF 640/580 ratio measured in vivo as shown in C. Plotted are 78 raw data points (gray circles) from 26 experiments. Mean SNARF ratio values (±SEM; black diamonds) for pH 6.8, 7.2, and 7.6 were 1.29 ± 0.02, 1.84 ± 0.05, and 2.52 ± 0.08, respectively. Solid line represents linear regression fit to the raw data, with slope = 1.6 ± 0.1 (s.d.) and intercept −9.89 ± 0.7 (s.d.), used to convert SNARF fluorescence ratio values to pH_i values in all subsequent experiments.

(as appropriate) to remove excess unloaded dye and then incubated at room temperature for ∼5–10 min to allow for recovery and de-esterification of loaded dye. The observed resting pH_i of SNARF-loaded cells was typically stable (∼7.2 as described below). Additionally, the rates and magnitudes of both cell shrinkage in response to CCh and cell swelling upon removal of agonist (as reported below) were nearly identical to values previously reported (Lee et al., 2007), suggesting that neither SNARF-loading nor illumination was significantly toxic to the cells over the time course of experiments (>20–40 min).

Ratiometric fluorescence measurements of pH_i were performed by sequential dual-emission imaging of SNARF fluorescence collected at ∼580 and ∼640 nm. Cells were illuminated with light from a Xe arc lamp filtered through a 480/40-nm band pass (bp) filter and reflected by a 515-nm long pass (lp) dichroic to the objective lens (40× Nikon Plan Fluor; 1.3 N.A.) for epi-illumination. Fluorescence emission collected by the objective was filtered sequentially with either a 580/10-nm bp filter or a 640/10-nm bp filter housed in a computer-controlled filter wheel (Sutter Instruments). DIC and fluorescence images were taken sequentially with a single camera using a method previously described (Foskett, 1988, 1990a) with a DIC polarizer/analyzer housed in the emission filter wheel (Lee et al., 2007). Light from a halogen lamp for DIC transillumination was filtered through a 610/10-nm bp filter and tested to ensure it did not pass through the two fluorescence emission filters or excite the SNARF dye. No measurable changes in background fluorescence and/or SNARF fluorescence were detected when high intensity 610-nm transmitted light was shuttered on and off with either the 580/10 or 640/10-nm emission filter in place. Three sequential images were taken at each time point (separated by ∼250–500 ms): (1) SNARF fluorescence image using 480/40-nm excitation and 580/10-nm emission filters; (2) SNARF fluorescence image using 480/40-nm excitation and 640/10-nm emission filters; (3) DIC image using filtered 610/10-nm transmitted light (Xe lamp shuttered closed) and DIC analyzer in the emission filter wheel. To minimize possible toxic effects of dye illumination, care was taken to minimize sampling frequency and both the illumination intensity (using neutral density filters) and length (exposure time) while still maintaining an acceptable signal to noise ratio (SNARF fluorescence >15-fold above background). Camera, image acquisition, and filter wheels were controlled by Perkin Elmer Ultraview LCI software.

To measure changes in $[Ca^{2+}]_i$, isolated serous acinar cells were loaded with 2 µM fura-2-AM (Molecular Probes) for ∼10–15 min using a procedure similar to that described above. Simultaneous DIC imaging of cell volume and fluorescence imaging of fura-2 as well as calibration of fura-2 340/380 ratios to $[Ca^{2+}]_i$ values were performed exactly as described previously (Lee et al., 2007). Cell volume determinations were estimated by taking the area of a DIC-imaged cross section of a serous cell or acini (traced using ImageJ software; W.S. Rasband, NIH, Bethesda, MD) to the 3/2 power, and cell volumes are expressed as normalized volumes (V) relative to the cell volume at $t = 0$ (V_o). We previously demonstrated that this method (Foskett, 1988, 1990a) provides a reproducible and accurate estimation of serous acinar cell volume when compared with cell volume measurements made via confocal 3-D reconstruction of fluorescent calcein-loaded serous cells (Lee et al., 2007).

Calibration of SNARF-5F in Murine Serous Acinar Cells

To quantitatively convert changes in SNARF 640/580 ratio to changes in pH_i, in vivo calibration experiments were performed to calibrate the behavior of the SNARF dye in serous acinar cells. The 640/580 fluorescence emission ratios were recorded from

SNARF-loaded cells exposed to the H^+/K^+ exchanger nigericin in solutions of high $[K^+]_o$ (to equilibrate $pH_i = pH_o$) with three different pH_o values (6.8, 7.2, and 7.6; example shown in Fig. 1 C). The linear regression fit of the raw data points taken from 17 calibration experiments (Fig. 1 D) was used to convert 640/580 ratios to pH_i values in all subsequent experiments. SNARF fluorescence varied linearly within the physiological pH_i range observed (Fig. 1 D).

Measurement of Intracellular Buffering Capacity

To convert changes in pH_i to rates of base equivalent (OH^- eq) flux, cellular buffering capacity had to first be taken into account. The total intracellular acid/base buffering capacity (β_T) is the sum of the CO_2–HCO_3^--dependent buffering capacity (β_{HCO3}) as well as the intrinsic CO_2-independent buffering capacity (β_i; including H^+-buffering of cytoplasmic macromolecules and organelles). Because of marked variation in buffering capacity of various cell types (due to size and organelle composition), β_i must be experimentally determined. Serous acinar cell β_i was measured by observing pH_i changes in cells and acini exposed to solutions of various $[NH_4Cl]_o$ in a Na^+- and HCO_3^--free solution to block pH_i regulatory mechanisms (as previously described in Roos and Boron, 1981; Renner et al., 1989; Weintraub and Machen, 1989). It has been demonstrated that exposure of cells to a solution of NH_3–NH_4^+ leads to rapid entry of membrane-permeant NH_3 into the cell, causing pH_i alkalinization reflective of H^+ consumption as the intracellular NH_3 is converted to NH_4^+. This is followed by a slower decrease in pH_i, believed to reflect NH_4^+ entry, possibly through K^+ channels and/or the Na^+/K^+ ATPase ((Boron and De Weer, 1976; for reviews see Roos and Boron, 1981; Thomas, 1984). Upon an experimental change in $[NH_3]_o$, the $[NH_4^+]_i$ can be calculated using the Henderson-Hasselbach relationship ($[NH_4^+]_i = [NH_3]_i \times 10^{pKa-pHi}$), assuming that $[NH_3]_i$ rapidly equilibrates with $[NH_3]_o$ and the pK_a of intracellular and extracellular NH_3/NH_4^+ is identical (~9.2; Weintraub and Machen, 1989).

Serous cells were exposed to solutions of 0, 5, 10, and 20 mM $[NH_4Cl]_o$ (representative experiment shown in Fig. 2 A), containing 0, 0.6, 1.2, and 2.5 mM $[NH_3]_o$, respectively, as calculated from Henderson-Hasselbach with $pH_o = 7.4$. After an experimental increase or decrease in $[NH_3]_o$, $[NH_4^+]_i$ was calculated at the point of initial fast pH_i increase or decrease. The mean buffering power of all non-NH_3–NH_4^+-dependent intracellular buffering (occurring around the midpoint of the pH_i change) was calculated as $\beta_i = \Delta[NH_4^+]_i/\Delta\ pH_i$ (in units of mmol·liter^{-1} of acid or base equivalent required to change pH_i by one unit). The raw data points taken from 24 β_i experiments (34 imaged acini/cells; Fig. 2 B, gray circles) were then fitted with an exponential function (Fig. 2 B; solid black line; as described in the legend).

The continuously gassed 5% CO_2–95% O_2-equilibrated solution clamps $[CO_2]_o$ constant, forming an open buffering system (for review see Roos and Boron, 1981; Boron, 2004). Because the plasma membrane is highly permeable to CO_2, it was assumed that $[CO_2]_i = [CO_2]_o = \sim 1.2$ mM (as determined by Henry's Law with $pCO_2 = 0.05$ atm). Using the Henderson-Hasselbach relationship and assuming that the intracellular pKa of CO_2–HCO_3^- is ~6.1 (Boron, 2004), $[HCO_3^-]_i = 1.2\ mM \times 10^{pHi-6.1}$ and $\beta_{HCO3-} = 2.3 \times [HCO_3^-]_i$ (Fig. 2 B, dashed line). Because $[CO_2]_i$ is constant, both $[HCO_3^-]_i$ and β_{HCO3-} rise exponentially as pH_i increases. Total intracellular pH buffering in the presence of CO_2-HCO_3^- was calculated as the sum of the two curves, $\beta_T = \beta_i + \beta_{HCO3-}$ (Fig. 2 B, u-shaped solid black line). For experiments performed in the absence of CO_2–HCO_3^-, it was assumed that intracellular pH_i buffering = β_i.

Measurement of OH^- Equivalent and Cl^- Fluxes

OH^- eq flux values for each experiment were determined by first using a median-smoothing filter to minimize noise in the raw

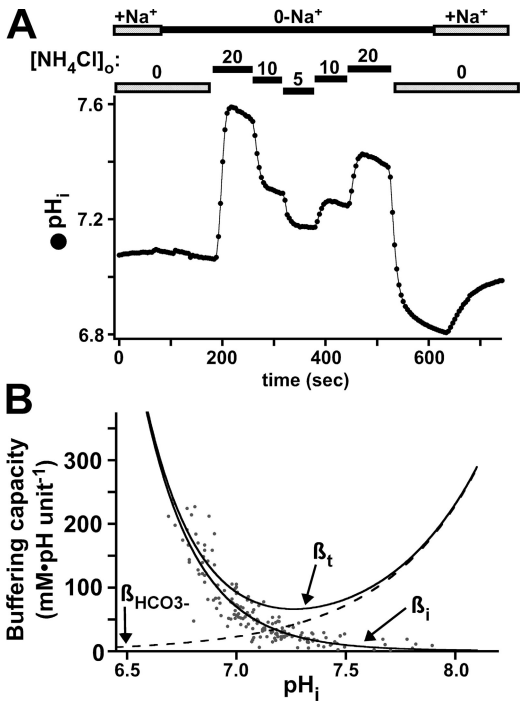

Figure 2. Measurement of serous acinar cell pH_i buffering capacity. (A) Representative NH_4Cl pulse experiment showing pH_i changes in response to varying $[NH_4Cl]_o$ (from 0 to 20 mM) in Na^+- and HCO_3^--free Solution E. Intrinsic cellular buffering capacity (β_i) was determined from NH_4Cl^--induced pH_i changes as described in Materials and methods. (B) Measurements of serous acinar cell β_i plotted as a function of pH_i. Data points (circles) represent 184 measurements made in 34 separate cells/acini from experiments as shown in A. Igor Pro software was used to fit β_i data with an exponential function (equation of fitted line: $\beta i = 0.88259 + 249.8 \cdot e^{((6.69-pHi)/0.243)}$). The dashed line represents CO_2–HCO_3^--dependent buffering (β_{HCO3-}), calculated as $2.3 \times [HCO_3^-]_i$ (as described in Materials and methods). The total buffering curve (β_t; u-shaped curve) is the sum of the β_i and β_{HCO3-} curves. Conversions of changes in pH_i to OH^- eq flux values were performed using either the β_t or β_i functions in the presence or absence of CO_2–HCO_3^-, respectively.

pH_i trace (Igor Pro Software; smoothing index = 3). Light median filtering best preserved the shape of the pH_i trace while removing single outlier points. The derivative of the smoothed pH_i trace was taken with respect to time (in units of pH unit·s^{-1}) for each point of the trace and then multiplied by the cellular buffering capacity (based on pH_i at that point) to obtain the OH^- eq flux (in units of meq OH^-·liter^{-1}·s^{-1}), which was then plotted vs. time.

Cl^- flux values were obtained by first converting relative cell volume values from each experiment to values of intracellular Cl^- content. As previously described (Foskett, 1990a,b, 1993), isosmotic loss of cellular KCl content is reflected in a parallel decrease in $[Cl^-]_i$ due to the presence of impermeant organic ions that make up >50% of cellular anionic content. The linear relationship between cell volume and $[Cl^-]_i$ in murine serous acinar cells was previously determined using the Cl^--sensitive fluorphore SPQ (Lee et al., 2007) and described by the linear fit $[Cl^-]_i$ (in mM) ≈ $((V/V_o) - 0.66)/0.005$. To determine CCh-stimulated Cl^- fluxes, the relationship between cell volume and actual Cl^- content lost by the cell was calculated from these data (i.e., the changes in cell volume must be taken into account). This transformation

TABLE II

Primers Used for rtPCR

Transcript	GenBank/EMBL/DDBJ accession number	Expected product (bp)		Primer set (5′ - 3′)	5′- binding site
NHE1	NM_016981	315	for	TGTAGAGTAGAAAGTACTG	4262
			rev	TGAAAAAGGTTCAGTTTCC	4558
NHE2	NM_001033289	127	for	CCATTTCTGTGTTTTTCCTG	3247
			rev	TCTTTAAACACTATGGGCTG	3354
NHE3	NM_001081060	207	for	AACTATGAAGAGATCAGTGG	2161
			rev	AGAGTTTGGAATCTGAACAC	2348
NHE4	NM_177084	223	for	TTGCTCTGGAGTTTAGTAAC	3566
			rev	TATTGATCTGGTTGCCATAG	3769
NHE5	NM_001081332	356	for	TCAGGAGTAGAGAATAGTAG	4763
			rev	CCTTTGTCTAGTAAATGCTC	5099
NHE6	NM_172780	385	for	GTGAAGAAATGTGTACTACC	2163
			rev	GTTTTTCCAACAAAGGAACC	2528
NHE7	NM_177353	403	for	GTGTATGATAATCAAGAGCC	2010
			rev	GAGTGGTAAGATAGTTTCAG	2384
NHE8	NM_148929	249	for	TTCTTTCTTCTCTGACATGG	4237
	NM_178371		rev	TAACTATCCAGTCATGTGAC	4466
NHE9	NM_177909	226	for	ACCTTATCACATGTATCCTC	2212
			rev	ATCCAAAATCCACATGAAGG	2418

assumed that resting $[Cl^-]_i$ = ~65 mM in SNARF-loaded acinar cells, as previously measured in SPQ-loaded acinar cells (65 ± 4 mM; Lee et al., 2007). The $[Cl^-]_i$ at each point (determined by the normalized cell volume) was multiplied by the normalized cell volume. For example, at rest, $[Cl^-]_i$ was ~65 mM. If V/V_o falls to 0.80, $[Cl^-]_i$ falls to ~28 mM, but because the Cl^- is contained in a smaller volume (the cell shrunk), the change in $[Cl^-]_i$ underestimates the actual amount of Cl^- content lost. Multiplying $[Cl^-]_i$ (28 mM) by volume (0.80) yields a Cl^- content of 22 mmol per liter of original (resting) cell volume (i.e., the cell lost 66 − 22 = ~44 mmol $Cl^- \cdot liter^{-1}$). Using the volume traces, normalized cell volume was multiplied by the $[Cl^-]_i$ at each point, and Cl^- flux was computed by taking the derivative of the Cl^- content trace with respect to time (in units of meq $Cl^- \cdot liter^{-1} \cdot s^{-1}$). Following electrophysiological convention, efflux of an anion across the plasma membrane out of a cell results in negative (inward) current, and thus negative Cl^- and OH^- eq flux values represent efflux of cellular Cl^- and OH^- equivalents.

Gene Expression Profiling of NHE Transcripts in Serous Acinar Cells

Gene expression profiling was performed as previously described ((Lee et al., 2007) using the method of (Van Gelder et al., 1990), for review see Eberwine, 2001). In brief, single small serous acini (three to four cells) plated on Cell-Tak–coated coverslips (washed several times to remove cellular and noncellular debris) were harvested by gentle suction with a pulled patch clamp glass electrode of ~5 µm diameter (taking care not to aspirate any debris). Two rounds of antisense RNA (aRNA) amplification were performed using a poly dT-oligo (to selectively amplify expressed mRNA) containing a T7 RNA polymerase promotor. Control RNA (from murine nasal turbinate, kidney, and brain) was extracted from surgically dissected tissue using TRIzol reagent (Invitrogen) according to the manufacturer's protocol. Due to the intrinsic 3′-biasing of aRNA amplification, primers were directed to the 3′ end of the published transcript sequences (~300–1,000 bp from the poly-A tail) obtained from GenBank/EMBL/DDBJ. Nonquantitative reverse transcription (rt)-PCR reactions were performed using a thermocycler and temperatures of 94°C, 57°C, and 72°C for denaturation, annealing, and extension steps, respectively. Reactions were run on a 1.8% agarose gel stained with ethidium bromide and visualized on a UV light box for photography. Transcript-specific primers and expected product sizes are listed in Table II. Four serous acinar aRNA samples and three parotid acinar aRNA samples from acini harvested from three different Wt C57BL/6 mice were used in these studies, as well as kidney, brain, and nasal turbinate RNA isolated from tissue taken from two different Wt C57BL/6 mice. No differences in tissue specific NHE transcript expression were observed between the mice. As controls, PCR reactions were performed on isolated RNA in which the reverse transcription (rt) step was omitted and no PCR products were detected (not depicted), suggesting that the results were reflective of RNA expression and not contaminating genomic DNA.

Immunocytochemistry and Confocal Immunofluorescence Microscopy

Isolated serous acinar cells and acini were plated on glass coverslips (coated with Cell-Tak) for ~30–45 min in Solution B. Cells and acini were then fixed with a solution of 4% formaldehyde in Dulbecco's PBS (DPBS; w/Ca^{2+} and Mg^{2+}; GIBCO BRL) for 20 min at room temp. Following aspiration of the fixative solution and three washes with DPBS (~5 min each), the coverslips were incubated for 1 h at room temp in DPBS containing 1% BSA, 1% normal goat serum, and 0.15% saponin. Primary antibody incubation was performed overnight at 4°C in the same solution. Anti-NHE1 antibody (NHE1-1A) was used at a final concentration of ~10 µg/ml. As a control for antibody specificity, NHE1 antigenic blocking peptide (NHE1-1P) was preincubated with 1° anti-NHE1 antibody at a concentration of 50 µg/ml (fivefold excess by weight) for ~1 h at 4°C. Polyclonal rabbit antiserum against NKCC1 (α-wCT; directed against the C terminus of rat NKCC1; Parvin et al., 2007) was used at a 1:300 dilution. Anti-CFTR monoclonal antibody 24-1 was used at a final dilution of 1:100. The specificity of CFTR immunostaining with 24-1 was previously demonstrated by use of serous acinar cells isolated from the *cftr*$^{tm1Unc-/-}$ mice and by inhibition of immunostaining by an antigen-containing C-terminal CFTR peptide (Lee et al., 2007).

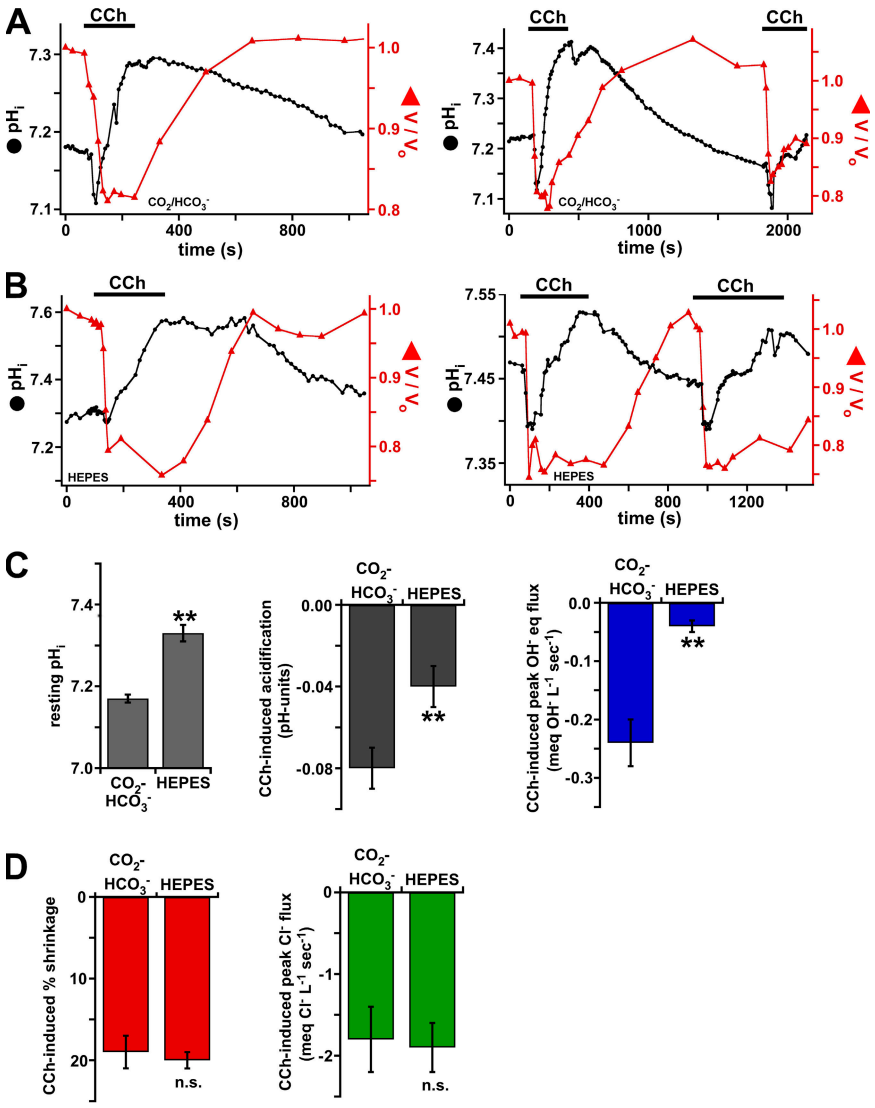

Figure 3. Serous acinar cell pH_i responses to CCh stimulation. (A) Representative experiments showing pH_i (black circles; left axes) and cell volume (red triangles; right axes) responses of SNARF-loaded serous acinar cells to stimulation with 100 µM CCh in CO_2–HCO_3^--buffered solution, showing transient acidification occurring concomitantly with CCh-induced cell shrinkage/Cl^- efflux followed by a prolonged alkalinization. Upon removal of agonist, pH_i relaxed back to near resting levels. A second identical response was observed upon reapplication of agonist (second panel). (B) Representative traces from cells stimulated with CCh in nominally CO_2–HCO_3^--free (HEPES-buffered) solution, resulting in ~50% smaller acidification (compared with CO_2–HCO_3^- conditions) but a similar subsequent pH_i increase. (C) Summary of resting pH_i (left), CCh-induced pH_i decrease (middle), and CCh-induced OH^- eq flux (right) in CO_2–HCO_3^-- and HEPES-buffered conditions. (D) Summary of cell shrinkage (left) and Cl^- fluxes (right).

Following 1° antibody incubation and three subsequent washes with DPBS, the coverslips were incubated in solution containing Alexa-Fluor (AF)–labeled 2° antibody (AF488 anti-mouse IgG, AF568 anti-rabbit IgG, or both as appropriate; Molecular Probes) for ~1–2 h at room temp. After three final washes in dPBS, the coverslips were mounted on slides using Vectashield mounting medium for fluorescence (Vector Laboratories) containing 1.5 µg/ml 4',6 diamidio-2-phenylindole (DAPI). Slides were stored in the dark at 4°C and viewed on an inverted Nikon microscope equipped with a 60× (1.4 N.A.; Nikon Plan Apochromat) objective lens. Immunofluorescent staining was visualized using the 488 and 568 lines of an Ar/Kr-ion laser attached to a Perkin Elmer Ultraview LCI spinning-disc confocal system. DAPI was visualized via wide-field fluorescence microscopy by moving a filter cube (containing a 400-nm lp dichroic mirror) into the light path to reflect light from a Xe-arc lamp (filtered through a 380/10-nm bp filter) to the specimen for epi-illumination. DAPI emission was collected and filtered through a 450-nm lp filter housed in the cube and detected by the same camera used for the confocal imaging.

Data Analysis

All data analysis and graphing was performed using Excel or Igor Pro Software (Wavemetrics, Inc.). Data are reported as mean ± SEM (s.e.m.) unless standard deviation (s.d.) is indicated. Image processing was performed using Perkin Elmer Ultraview Software and/or ImageJ. Statistical significance/P values were determined using Student's two-tailed *t* test. A P value of <0.05 was considered statistically significant. For all bar graphs, a single asterisk represents $P < 0.05$, a double asterisk represents $P < 0.01$, and n.s. represents no statistical significance.

RESULTS

CCh Stimulation of Isolated Serous Acinar Cells Causes a Transient Acidification that Is Reduced in the Absence of CO_2–HCO_3^-

Serous acinar cells loaded with the pH_i probe SNARF-5F exhibited a resting pH_i of 7.17 ± 0.01 ($n = 51$) in 5% CO_2–25 mM HCO_3^--buffered medium (Solution A) that remained stable in most cells for >30–45 min of observation. Cells and acini that initially exhibited a slowly drifting or unstable pH_i (~15% of cells) were allowed to equilibrate for 3–5 min without illumination. Typically, a steady-state pH_i near 7.2 was observed after this

rest period, and these cells/acini were used for experiments. However, cells that did not reach a steady-state pH_i after 3–5 min (<5% of all observed cells) were discarded. No differences were observed in the responses of cells with a preliminary slight pH_i drift and an immediately stable resting pH_i.

SNARF-loaded serous acinar cells and acini stimulated with 100 μM CCh in CO_2–HCO_3^- medium exhibited a marked decrease in cell volume of 19 ± 2% within 70 ± 11 s (n = 9) that reversed upon removal of agonist to >95% resting volume after 310 ± 52 s (n = 9; Fig. 3 A). These responses were similar to previously reported observations (Lee et al., 2007), suggesting that SNARF loading was not toxic to Cl^- efflux and influx pathways previously characterized. Additionally, CCh stimulated a transient pH_i decrease (acidification) of 0.08 ± 0.01 pH units within 49 ± 6 s (n = 9) that occurred concomitantly with the cell shrinkage (Fig. 3 A). This was followed immediately by an alkalinization above the resting pH_i level (7.35 ± 0.02; n = 10). Upon washout of agonist, pH_i returned to near resting levels within 500 ± 90 s and remained stable until subsequent restimulation (Fig. 3 A, second panel). In nominally CO_2–HCO_3^--free solution (Solution B, buffered with HEPES and gassed with 100% O_2), the cells exhibited an alkalinized resting pH_i (7.33 ± 0.02; n = 37; Fig. 3, B and C), likely due to the lack of intracellular H^+ formed by the reaction of dissolved CO_2 with H_2O to form H_2CO_3 (which dissociates to HCO_3^- and H^+). Serous cells in CO_2–HCO_3^--free buffer exhibited a CCh-induced acidification of 0.03 ± 0.01 pH units (n = 10; Fig. 3, B and C), smaller than the acidification observed in CO_2–HCO_3^- buffer ($P < 0.01$). However, the time to peak acidification (59 ± 9 s) was not different. In contrast to the reduced initial acidification, the subsequent CCh-induced alkalinization remained intact in the absence of CO_2–HCO_3^-, as pH_i increased to 7.47 ± 0.05 (n = 9). No differences were observed in the magnitude or rate of CCh-induced cell shrinkage (20 ± 1% within 74 ± 7 s; n = 8) or cell swelling upon CCh removal (time to return to >95% V_o = 297 ± 44 s; n = 8) in HEPES-buffered conditions compared with CO_2–HCO_3^--buffered conditions. These results are summarized in Fig. 3 (C and D) and suggest that CO_2–HCO_3^- is required for maximal CCh-induced acidification, but not for the activation of the observed alkalinization mechanism nor for either normal cell shrinkage (Cl^- efflux) or cell swelling (Cl^- influx).

Serous acinar cell buffering capacity measurements were performed to enable extrapolation of pH_i changes to magnitudes of base equivalent (OH^- eq) fluxes (Fig. 2). In CO_2–HCO_3^--containing medium, the peak net OH^- eq flux during CCh-induced acidification was −0.23 ± 0.04 meq·liter^{-1}·s^{-1} (n = 11; Fig. 3 C). This peak OH^- eq flux coincided with the peak CCh-induced net Cl^- flux of −1.8 ± 0.4 meq·liter^{-1}·s^{-1} (n = 11; Fig. 3 D). Confirming the similar kinetics of the initial CCh-induced acidification and cell shrinkage (as shown in the traces in Fig. 3), the peak OH^- eq and Cl^- fluxes occurred concomitantly, at 19 ± 2 and 17 ± 2 s, respectively (n.s.), after the onset of cell shrinkage. In HEPES-buffered conditions, the initial OH^- eq flux during CCh stimulation was −0.04 ± 0.01 meq·liter^{-1}·s^{-1}, equivalent to only ∼19% of the flux observed in CO_2–HCO_3^--buffered conditions ($P < 0.01$). In contrast, the CCh-induced peak Cl^- flux in HEPES buffer (−1.9 ± 0.3 meq·liter^{-1}·s^{-1}; Fig. 3 D) was identical to that observed in CO_2–HCO_3^- buffer (n.s.). As observed in CO_2–HCO_3^-, the peak CCh-induced Cl^- and OH^- eq fluxes occurred concomitantly, at 20 ± 4 and 22 ± 4 s, respectively, after the onset of cell shrinkage. These values were not different from each other or those observed in CO_2–HCO_3^- buffer. These results demonstrate that the CCh-induced OH^- eq flux during the initial CCh-induced acidification was strongly CO_2–HCO_3^--dependent. In contrast, the Cl^- efflux underlying the CCh-induced cell shrinkage was unaffected by the presence or absence of CO_2–HCO_3^-.

Inhibition of Na^+/H^+ Exchange Increases the Magnitude of and Prolongs the CCh-induced Acidification

The marked alkalinization subsequent to the rapid transient CCh-induced acidification suggested that, in addition to the initial CCh-induced net OH^- eq efflux, an alkalinization mechanism is also activated during CCh stimulation. The most ubiquitous cellular pH_i control mechanism is plasma membrane Na^+/H^+ exchange, mediated primarily by the SLC9A family of Na^+/H^+ exchange proteins (NHEs; for reviews see Orlowski and Grinstein, 2004; Zachos et al., 2005). At least 10 NHE isoforms have been cloned from mammalian cells (for review see Orlowski and Grinstein, 2004). The main plasma membrane NHE isoforms (NHE1–5 and possibly 8) are believed to operate with an electroneutral 1:1 Na^+:H^+ stoichiometry. NHE1 is ubiquitous, where it plays a crucial role in pH_i homeostasis (for review see Masereel et al., 2003). In addition, NHEs can have specialized roles in secretory and absorptive epithelia, including sustaining secondarily active Cl^- secretion (via basolateral NHE1 activity in concert with basolateral Cl^-/HCO_3^- [anion] exchange [AE], as observed in parotid acinar cells; Robertson and Foskett, 1994; for review see Melvin et al., 2005) and mediating H^+ secretion and/or Na^+ absorption (via apical NHE2 and/or NHE3 activity, as observed in the gastrointestinal tract and kidney; for review see Zachos et al., 2005). Because of their ubiquitous nature, as well as evidence that NHE activity is up-regulated upon muscarinic stimulation in exocrine acinar cells from parotid gland (Robertson and Foskett, 1994; Robertson et al., 1997; Evans et al., 1999; Park et al., 2001), pancreas (Brown et al., 2003), and sublingual mucous glands (Nguyen et al., 2000), we hypothesized that CCh-induced NHE activity mediated the sustained

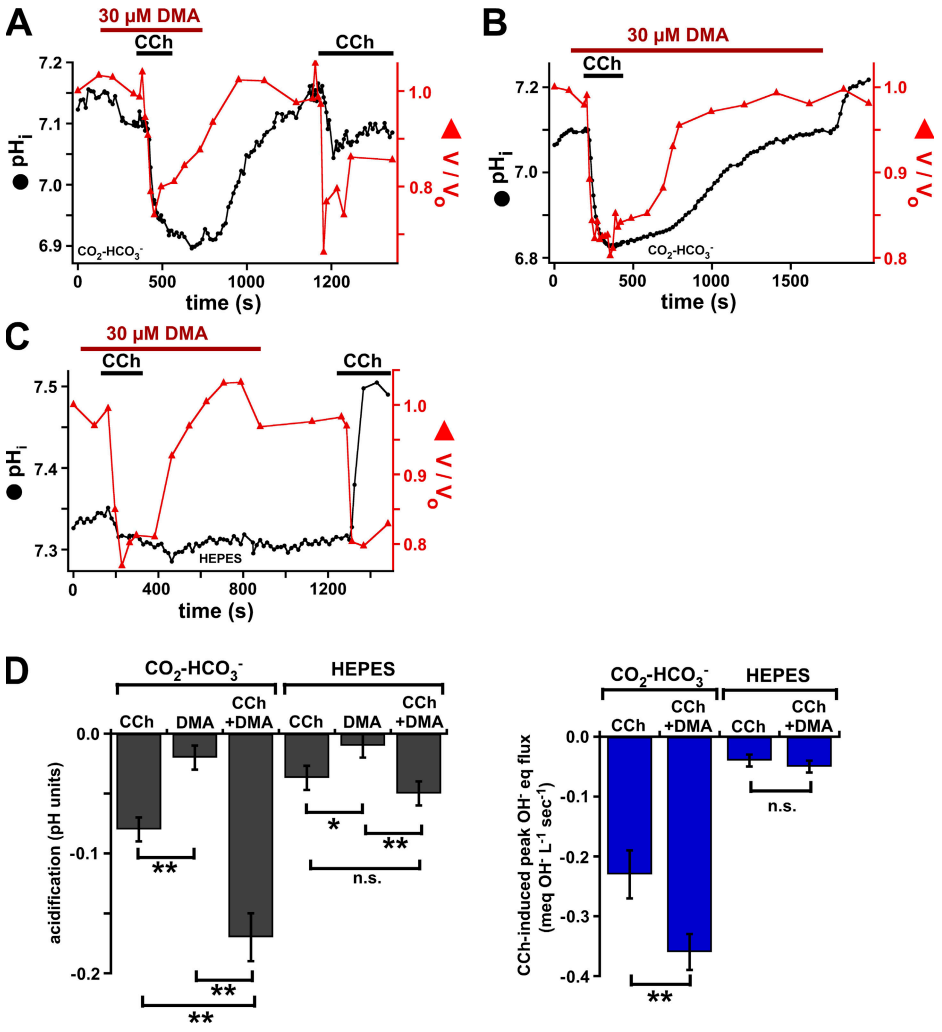

Figure 4. DMA enhances and prolongs CCh-induced acidification. (A) Representative experiment showing enhanced and prolonged CCh-induced acidification in serous acinar cells exposed to 30 μM DMA in presence of CO_2–HCO_3^-. (B) After removal of CCh, 30 μM DMA significantly slowed pH_i recovery but did not affect cell swelling (Cl^- uptake). (C) Serous cells in CO_2–HCO_3^--free conditions stimulated with CCh in the presence of DMA exhibited small acidification nearly identical to that observed in DMA-free conditions. However, DMA strongly blocked the subsequent pH_i increase observed in presence of CCh alone. (D) Summary comparing CCh-induced acidification (left) and OH^- eq flux data (right) ± 30 μM DMA in CO_2–HCO_3^-- and HEPES-buffered conditions.

alkalinization observed upon prolonged stimulation of serous acinar cells.

The amiloride-derivative 5-(*N*,*N*-dimethyl)amiloride (DMA) is a potent inhibitor of NHE activity (for review see Masereel et al., 2003). We previously showed that 30 μM DMA (a saturating concentration for many NHE isoforms) affected neither CCh/Ca^{2+}-induced cell shrinkage (Cl^- secretion) nor cell swelling (Cl^- uptake) upon restoration of resting $[Ca^{2+}]_i$ (Lee et al., 2007). This suggests that paired NHE/AE activity is not critical for maintenance of Cl^- secretion in airway gland serous cells, in contrast with the important role these proteins serve in sustaining parotid gland Cl^- secretion (Robertson and Foskett, 1994). The effects of DMA on agonist-induced pH_i changes were measured in SNARF-loaded serous acinar cells. Exposure of cells to 30 μM DMA alone had little affect on resting pH_i, resulting in a maximal acidification of only 0.02 ± 0.01 pH units in CO_2–HCO_3^- buffer ($n = 6$) and 0.01 ± 0.01 pH units in HEPES buffer ($n = 14$) after prolonged (>300 s) exposures. In contrast to its minimal effect on resting pH_i, DMA strongly enhanced the CCh-induced acidification in CO_2–HCO_3^- buffer. After ~60–100 s pretreatment with 30 μM DMA, acinar cells were stimulated with 100 μM CCh in the continued presence of DMA. CCh caused pH_i to drop by 0.17 ± 0.02 pH units ($n = 8$; Fig. 4 A, summarized in D), a greater than twofold increase compared with CCh stimulation in the absence of DMA ($P < 0.01$). The peak CCh-induced OH^- eq flux in the presence of DMA (−0.36 ± 0.03 meq·liter^{-1}·s^{-1}; $n = 8$) was also increased compared with that observed during stimulation with CCh alone ($P < 0.05$; Fig. 4 D). Additionally, DMA treatment profoundly inhibited the alkalinization that typically followed the transient CCh-induced acidification (compare Fig. 4 A with Fig. 3 A) and substantially slowed pH_i recovery after removal of CCh (Fig. 4 B), as described in more detail below.

In contrast, the small CCh-induced acidification in HEPES-buffered solution was not enhanced by the presence of 30 μM DMA (0.05 ± 0.01 pH units; $n = 14$; Fig. 4 C, summarized in D). In HEPES buffer, the peak CCh-induced OH^- eq flux in the presence DMA (−0.05 ± 0.01 meq·liter^{-1}·s^{-1}; $n = 14$) was also not different compared with that observed in the absence of DMA (summarized

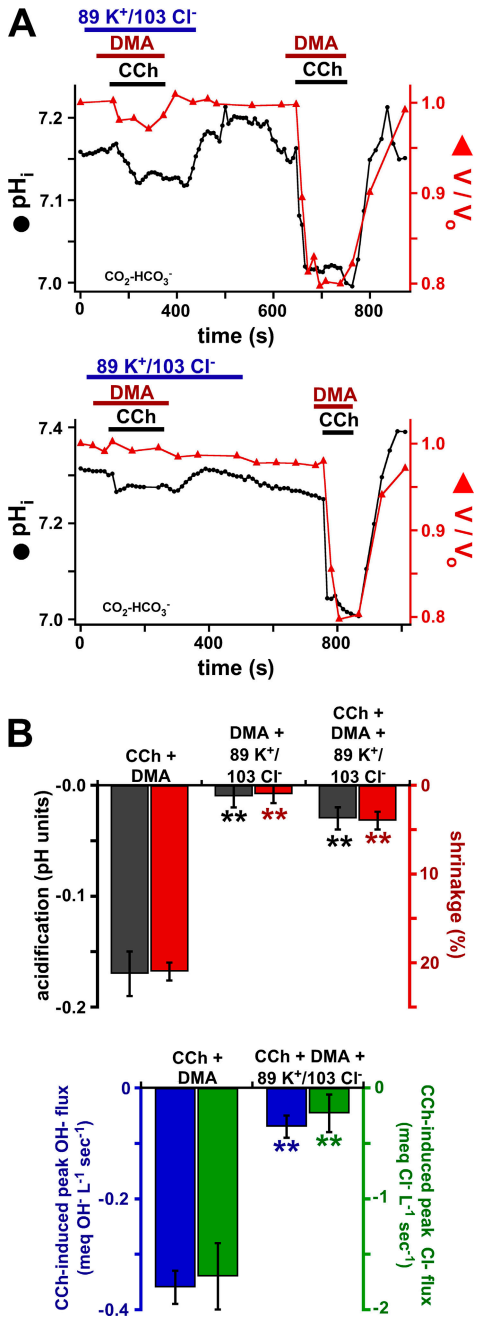

Figure 5. Blocking the driving force for conductive HCO_3^- efflux significantly inhibits CCh/DMA-induced acidification. (A) Representative experiments showing serous acinar cells stimulated with 100 μM CCh after pretreatment with 30 μM DMA in high (89 mM) $[K^+]_o$/low (103 mM) $[Cl^-]_o$ conditions (Solution G), demonstrating that both cell shrinkage and acidification are blocked under these conditions. (B) Mean CCh-induced pH_i decrease and cell shrinkage (top graph) along with peak CCh-induced OH^- eq and Cl^- fluxes (bottom graph) in Solution A (normal $[K^+]_o$/$[Cl^-]_o$) vs. Solution G (high $[K^+]_o$/low $[Cl^-]_o$). Asterisks represent significance when compared with 100 μM CCh stimulation in Solution A in the presence of 30 μM DMA.

in Fig. 4 D). However, the subsequent alkalinization observed after the transient initial CCh-induced drop (as seen in Fig. 3 B) was totally absent in the presence of DMA (Fig. 4 B), suggesting that NHE mediates the prolonged alkalinization during CCh stimulation in the absence of CO_2–HCO_3^-. In agreement with previous observations that DMA did not affect secretagogue-induced Cl^- content dynamics, neither CCh-induced cell shrinkage nor the CCh-induced peak Cl^- flux was affected by DMA. In CO_2–HCO_3^- buffer in the presence of DMA, cells shrunk by 21 ± 1% within 72 ± 11 s with a peak Cl^- flux of -1.7 ± 0.3 meq·liter^{-1}·s^{-1} ($n = 8$), values nearly identical to those measured during CCh stimulation in the absence of DMA. The presence of DMA also had no effect on CCh-induced cell shrinkage in HEPES buffer (20 ± 1% within 76 ± 7 s) or peak CCh-induced Cl^- flux (-1.5 ± 0.1 meq·liter^{-1}·s^{-1}; $n = 14$). DMA did not affect the similar initial kinetics of cell shrinkage and acidification in either buffer, as evidenced by the traces in Fig. 4. In CO_2–HCO_3^-, the initial peak OH^- eq flux and Cl^- flux occurred concomitantly at 17 ± 5 and 16 ± 3 s, respectively, after the onset of cell shrinkage. Identical observations were made in HEPES buffer, with peak OH^- and Cl^- fluxes occurring at 19 ± 3 and 17 ± 7 s after the onset of cell shrinkage (n.s. compared with each other and compared with values in CO_2–HCO_3^- buffer).

These data suggest that NHE activity is up-regulated during CCh stimulation of serous acinar cells, which minimizes the magnitude of the initial acidification present in CO_2–HCO_3^--containing medium and causes the subsequent CO_2–HCO_3^--independent alkalinization. Before further investigation of this CCh-activated NHE-mediated alkalinization (as described below), we first determined whether the initial CCh-induced net OH^- eq efflux underlying the observed acidification was indeed caused by an efflux of cellular HCO_3^- content reflective of HCO_3^- secretion.

Reducing the Driving Force for HCO_3^- Efflux Blocks CCh-induced Acidification

To test if CCh-induced acidification was caused by HCO_3^- efflux, ion substitution was used to eliminate the driving force for HCO_3^- movement, and the subsequent effects on CCh-induced pH_i changes were observed. At the resting pH_i of ~7.2, with $[HCO_3^-]_i$ = ~16 mM and $[HCO_3^-]_o$ = 25 mM, the Nernst equilibrium potential for HCO_3^- (E_{HCO3-}) = ~−12 mV. Therefore, with the cell membrane potential (V_m) = E_{HCO3-} = −12 mV, the driving force for net HCO_3^- flux should be eliminated. Since stimulation of serous cells with CCh was previously shown to result in net efflux of a large quantity (>40 meq liter^{-1}) of cellular KCl (Lee et al., 2007), it was assumed that K^+ and Cl^- permeabilities are dominant in setting V_m during CCh stimulation, and that changing $[K^+]_o$ and $[Cl^-]_o$ so both E_K and E_{Cl} = −12 mV would clamp V_m at −12 mV and abrogate the driving force for conductive HCO_3^- efflux. The mean resting $[Cl^-]_i$ was previously determined to be ~65 ± 4 mM

in serous acinar cells (Lee et al., 2007). While not directly measured, $[K^+]_i$ was assumed to be ~140 mM, a typical $[K^+]_i$ value as measured in other mammalian cells (for review see Foskett, 1990b). Thus under normal conditions ($[Cl^-]_o$ = 135 mM; $[K^+]_o$ = 5 mM), E_{Cl} = ~−19 mV and E_K = ~−87 mV. From the Nernst equation, it was calculated that lowering $[Cl^-]_o$ to 103 mM and raising $[K^+]_o$ to 89 mM would set $E_{Cl} = E_K = E_{HCO3}$ = −12 mV.

Serous acinar cells were stimulated with 100 µM CCh in the presence of 30 µM DMA (to accentuate the observed CCh-induced acidification by blocking subsequent NHE-mediated alkalinization) in CO_2–HCO_3^--buffered solution containing 103 mM $[Cl^-]_o$ and 89 mM $[K^+]_o$ (Solution G; Fig. 5 A). The maximal CCh-induced acidification in high $[K^+]_o$/low $[Cl^-]_o$ buffer + DMA was 0.032 ± 0.008 pH units (n = 10), and the maximal CCh-induced OH^- eq flux was −0.07 ± 0.02 meq·liter^{-1}·s^{-1} (n = 10; summarized in Fig. 5 B). These values are both ~80% smaller than those observed during CCh stimulation in normal $[K^+]_o$/$[Cl^-]_o$ CO_2–HCO_3^- buffer in the presence of DMA ($P < 0.01$ for both). Additionally, cell shrinkage was also almost completely blocked, as expected since $[K]_i \cdot [Cl]_i = [K]_o \cdot [Cl]_o$ and thus the driving force for KCl efflux had been nearly eliminated. Maximal CCh-induced shrinkage was reduced to 3 ± 1% with maximal Cl^- flux of −0.23 ± 0.17 meq·liter^{-1}·s^{-1} (n = 10; summarized in Fig. 5 B). These measurements correspond to ~84% and 86% inhibition, respectively, compared with observations during CCh stimulation in the presence of DMA in normal $[K^+]_o$/$[Cl^-]_o$ buffer ($P < 0.01$ for both). These results indicate that CCh-induced acidification requires conductive efflux of cellular HCO_3^-, suggesting that the acidification reflects cholinergic-stimulated HCO_3^- secretion occurring concomitantly with Cl^- secretion.

CFTR Is Not Required for CCh-induced Acidification

The above data demonstrate that CCh stimulation is associated with an efflux of HCO_3^- from serous acinar cells. We considered the possibility that this may occur through the same permeability that mediates the CCh-induced Cl^- efflux. We previously demonstrated that CCh-induced Cl^- efflux does not depend on CFTR, as it was not reduced in acinar cells isolated from *cftr*$^{tm1Unc-/-}$ knockout mice (lacking functional CFTR; for review see Grubb and Boucher, 1999) or in acinar cells exposed to the CFTR inhibitor $CFTR_{inh}$172 (Lee et al., 2007). To now examine whether CCh-induced HCO_3^- efflux requires CFTR function, we again used acinar cells isolated from the *cftr*$^{tm1Unc-/-}$mice. Acinar cells isolated from *cftr*$^{tm1Unc-/-}$mice stimulated with 100 µM CCh in the presence of 30 µM DMA were observed to shrink robustly (21 ± 2%) with a peak CCh-induced Cl^- efflux of −2.2 ± 0.2 meq Cl^- liter^{-1} s^{-1} (n = 9; unpublished data). Shrinkage was accompanied by an acidification of 0.20 ± 0.02 pH units with a peak CCh-induced OH^- eq flux of −0.31 ± 0.05 meq OH^- liter^{-1} s^{-1} (n = 10; unpublished data). These values were not different from those observed

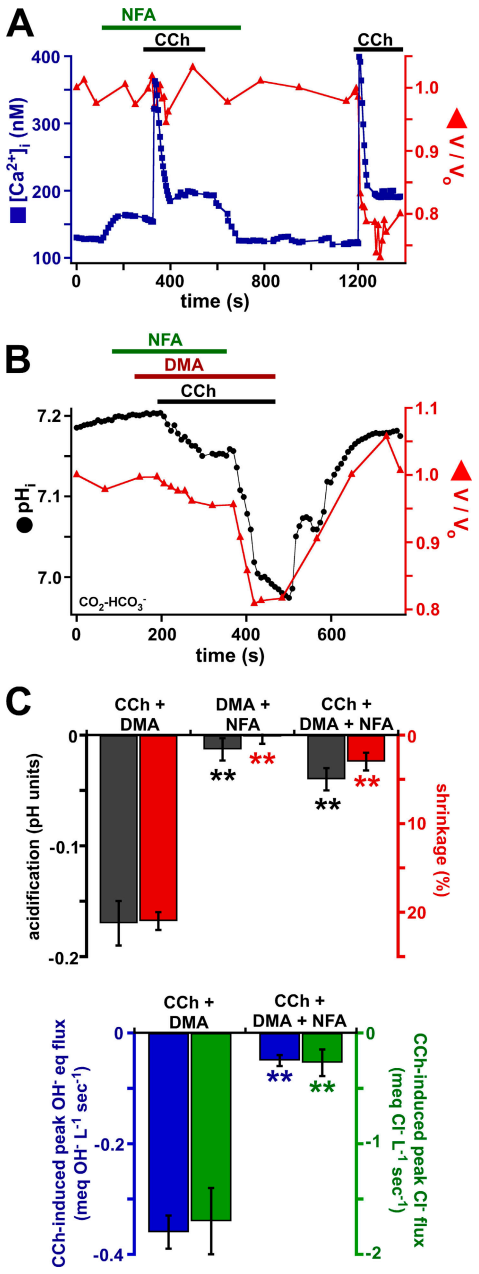

Figure 6. NFA inhibits CCh/DMA-induced acidification and cell shrinkage/Cl^- efflux, suggesting that both Cl^- and HCO_3^- effluxes occur through a similar Cl^- channel pathway. (A) Representative experiment showing that application of 100 µM NFA completely blocked CCh-induced cell shrinkage/Cl^- efflux without significantly inhibiting CCh-induced $[Ca^{2+}]_i$ signals. (B) Representative experiment showing that NFA blocks CCh-induced acidification (~80%) in the presence of 30 µM DMA. NFA inhibited cell shrinkage to a similar extent. (C) Summary of acidification and cell shrinkage (top) along with peak CCh-induced Cl^- and OH^- eq fluxes (bottom). Asterisks represent significance compared with 100 µM CCh stimulation in the presence of 30 µM DMA but in the absence of NFA.

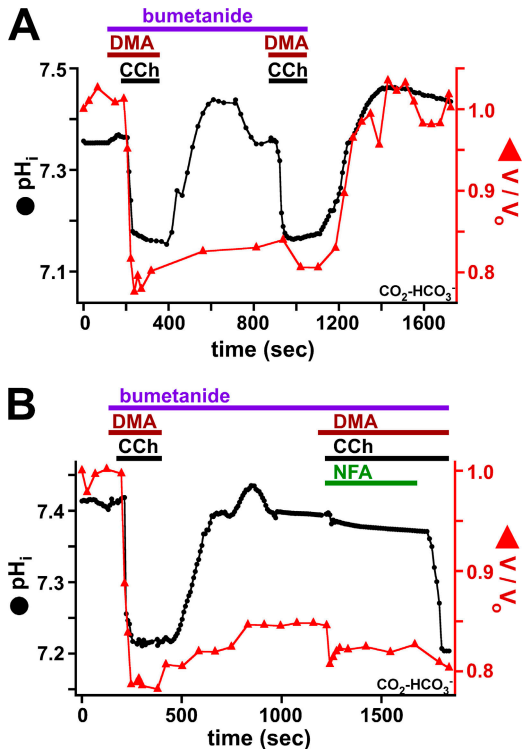

Figure 7. Inhibition of NKCC does not affect CCh-induced pH_i dynamics, suggesting that CCh/DMA-induced acidification is not dependent on changes in $[Cl^-]_i$ and that NFA block of HCO_3^- efflux is not dependent on block of Cl^- efflux. (A) Recovery of pH_i after CCh + DMA-induced acidification was not dependent on influx of Cl^- (cell swelling; blocked with 100 µM bumetanide). (B) Representative experiment showing NFA inhibition of CCh + DMA-induced acidification under conditions of low $[Cl^-]_i$ (shrunken cell with Cl^- uptake inhibited by bumetanide).

in Wt acinar cells (as reported above), suggesting that CFTR does not contribute to either the magnitude or rate of CCh-induced Cl^- or HCO_3^- efflux.

The Cl^- Channel Blocker Niflumic Acid Strongly Inhibits both CCh-induced Cell Shrinkage/Cl^- Efflux and CCh-induced Acidification/HCO_3^- Efflux

Because CCh-induced loss of Cl^- (Lee et al., 2007) or HCO_3^- content does not depend on CFTR, we hypothesized that another Cl^- channel, possibly a Ca^{2+}-activated Cl^- channel, serves as the Cl^- efflux pathway during cholinergic stimulation. The nonspecific Cl^- channel blocker NFA inhibits several types of heterologously expressed and endogenous Ca^{2+}-activated Cl^- currents (for review see Hartzell et al., 2005) and inhibits CCh-evoked fluid secretion from intact murine submucosal glands (Ianowski et al., 2007). We therefore examined the effects of NFA on both agonist-induced Cl^- secretion and acidification. We hypothesized that NFA inhibition of the secretory Cl^- channel would block agonist-induced cell shrinkage as well as OH^- eq efflux. First, however, control experiments were performed to examine whether NFA interfered with CCh-triggered Ca^{2+} signaling.

Serous cells loaded with fura-2 exhibited a 100 µM CCh-induced peak $[Ca^{2+}]_i$ of 468 ± 57 nM followed by a plateau $[Ca^{2+}]_i$ of 177 ± 17 nM (n = 10; unpublished data) in the absence of NFA (control conditions). The presence of either 10 or 100 µM NFA had no effect on these $[Ca^{2+}]_i$ levels. The CCh-induced peak and plateau $[Ca^{2+}]_i$ values were 397 ± 37 and 182 ± 11 nM, respectively, in the presence of 10 µM NFA (n = 9) and 431 ± 61 and 188 ± 60 nM, respectively, in the presence of 100 µM NFA (n = 5; Fig. 6 A). Nevertheless, while the CCh-induced increase in $[Ca^{2+}]_i$ was accompanied by a 20 ± 2% shrinkage within 62 ± 8 s (n = 6) in the absence of NFA, the magnitude and rate of CCh/Ca^{2+}-induced cell shrinkage was reduced to 15 ± 2% within 85 ± 6 s in the presence of 10 µM NFA (n = 8; $P < 0.05$ for both values). CCh-induced cell shrinkage/Cl^- efflux was nearly completely inhibited with 100 µM NFA (Fig. 6 A; max shrinkage = 4 ± 2%; n = 5; $P < 0.01$ compared with control), despite the robust CCh-evoked $[Ca^{2+}]_i$ response. These observations indicate that NFA blocks Cl^- efflux without inhibiting the CCh/muscarinic receptor Ca^{2+} signal, suggesting that NFA directly inhibits the secretory Cl^- channel.

Exposure of acinar cells to 100 µM NFA + 30 µM DMA (to magnify any observed acidification) in the absence of CCh had little effect on either pH_i or cell volume (Fig. 6 C). The maximal observed acidification was 0.01 ± 0.01 pH units and maximal observed shrinkage was 0 ± 1% (n = 7) after prolonged (>300 s) exposure. When acinar cells were stimulated with 100 µM CCh in the presence of both 30 µM DMA and 100 µM NFA, both cell shrinkage and acidification were severely reduced (Fig. 6 B, summarized in C). CCh caused pH_i to fall by only −0.04 ± 0.01 pH units with a peak OH^- eq flux of −0.05 ± 0.01 meq OH^-·liter^{-1}·s^{-1} (n = 7). This corresponded to ∼76% and 86% inhibition of the acidification and OH^- eq flux, respectively, compared with CCh + DMA application in the absence of NFA ($P < 0.01$ for both). NFA also reduced CCh-induced cell shrinkage (4 ± 1%) and peak Cl^- flux (−0.27 ± 0.12 meq Cl^-·liter^{-1}·s^{-1}; n = 7). This corresponded to ∼80% and ∼84% inhibition, respectively, compared with CCh application in the presence of DMA alone ($P < 0.01$ for both values; summarized in Fig. 6 C). The identical magnitudes of the effects of NFA on HCO_3^- and Cl^- effluxes suggest they occur through a similar Cl^- channel pathway.

Block of HCO_3^- Efflux by NFA Is Not a Secondary Effect of Blocking Cl^- Efflux

Another possible interpretation of the NFA inhibition of the CCh-induced acidification is that the normal fall in $[Cl^-]_i$ caused by CCh stimulation provides a driving force for HCO_3^- efflux through a Cl^-/HCO_3^- exchanger, and that NFA blocks the apparent HCO_3^- efflux indirectly by blocking Cl^- channel-mediated Cl^- efflux. However, this mechanism seems unlikely due to the

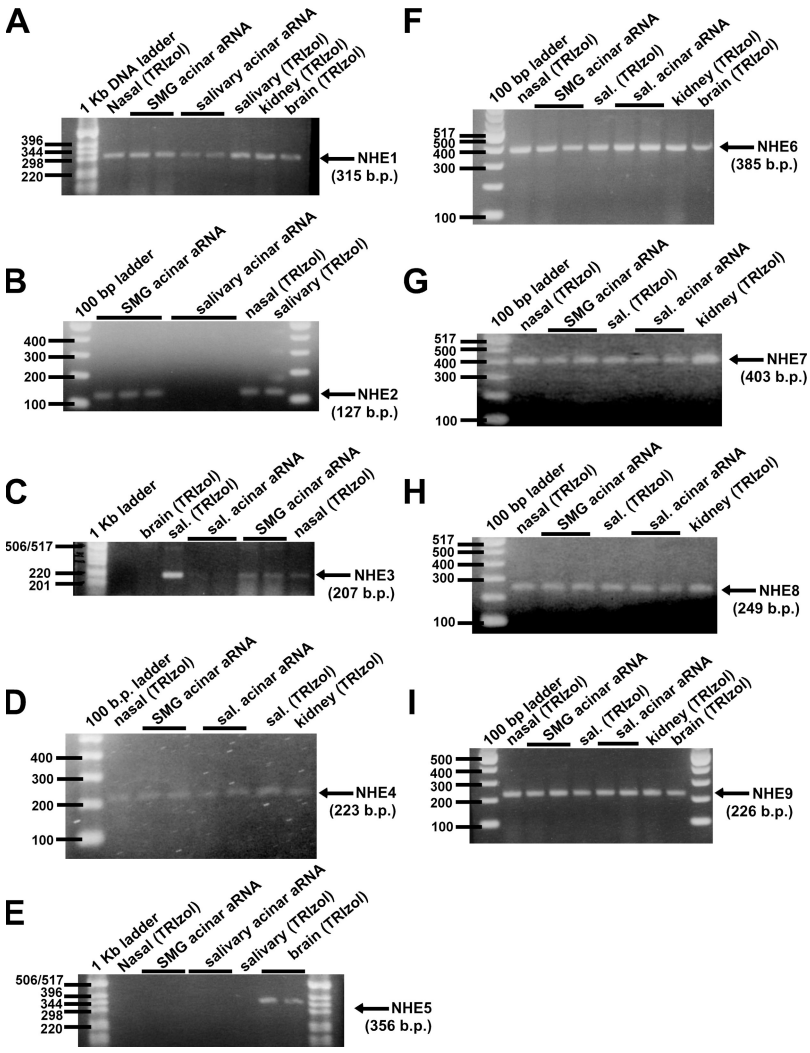

Figure 8. NHE isoform mRNA transcript expression in murine airway gland serous acinar cells. Messenger RNAs harvested from small airway gland serous acini were amplified and subject to rtPCR using NHE isoform-specific primers (shown in Table II). (A–I) Representative EtBr-stained agarose gels showing PCR products demonstrating expression of NHE isoforms 1–9. Serous acinar cells (SMG acinar aRNA) expressed NHEs 1, 2, 3, 4, 7, 8, and 9. These isoforms were also detected in RNA isolated from nasal tissue.

reproducible kinetic correspondence of the CCh-induced acidification (HCO_3^- efflux) and cell shrinkage (Cl^- efflux). Nevertheless, to rule out a dependence of CCh-induced OH^- eq efflux on the Cl^- gradient, we examined the effect of NFA on pH_i in cells with reduced $[Cl^-]_i$. Serous acinar cells were stimulated with 100 μM CCh in the presence of 30 μM DMA and 100 μM bumetanide (Fig. 7 A), the latter to block NKCC1-mediated Cl^- uptake (as previously shown in Lee et al., 2007). Following removal of CCh and DMA, pH_i returned to resting levels (time to 50% pH_i recovery 190 ± 40 s; $n = 4$), but bumetanide prevented Cl^- uptake and volume recovery. Under these conditions, $[Cl^-]_i$ was ∼30 mM, as demonstrated previously (Lee et al., 2007). Restimulation of the shrunken $[Cl^-]_i$-depleted cells with CCh in the presence of 30 μM DMA led to another acidification that was similar to that associated with the first stimulation. This second acidification was nearly completely blocked by 100 μM NFA (Fig. 7 B; representative of three experiments), demonstrating that NFA inhibits agonist-induced acidification even under conditions of low $[Cl^-]_i$. These results strongly suggest that the block of HCO_3^- efflux by NFA is a direct effect, and not a secondary effect of blocking the concomitant Cl^- efflux.

Expression of NHE isoform mRNA Transcripts in Serous Acinar Cells

Taken together, the above data suggest that CCh stimulation induces an acidification caused by a net loss of OH^- equivalents reflecting secretion of HCO_3^- though a Cl^- channel pathway. Because CCh also caused a prolonged DMA-sensitive alkalinization following the immediate acidification, we hypothesized that NHE could function as a mechanism to maintain HCO_3^- efflux by extruding protons and alkalinizing pH_i during sustained secretion (i.e., activated Cl^- and HCO_3^- efflux pathways). Because $[CO_2]_i$ is clamped equal to $[CO_2]_o$ as a consequence of the high membrane permeability to CO_2, this alkalinization would promote the hydration of CO_2 to carbonic acid, which would then dissociate to form HCO_3^- and H^+ (for reviews see Roos and Boron, 1981; Boron, 2004), keeping $[HCO_3]_i$ elevated. To determine which NHE isoform(s) are responsible for alkalinizing pH_i during muscarinic stimulation, and whether

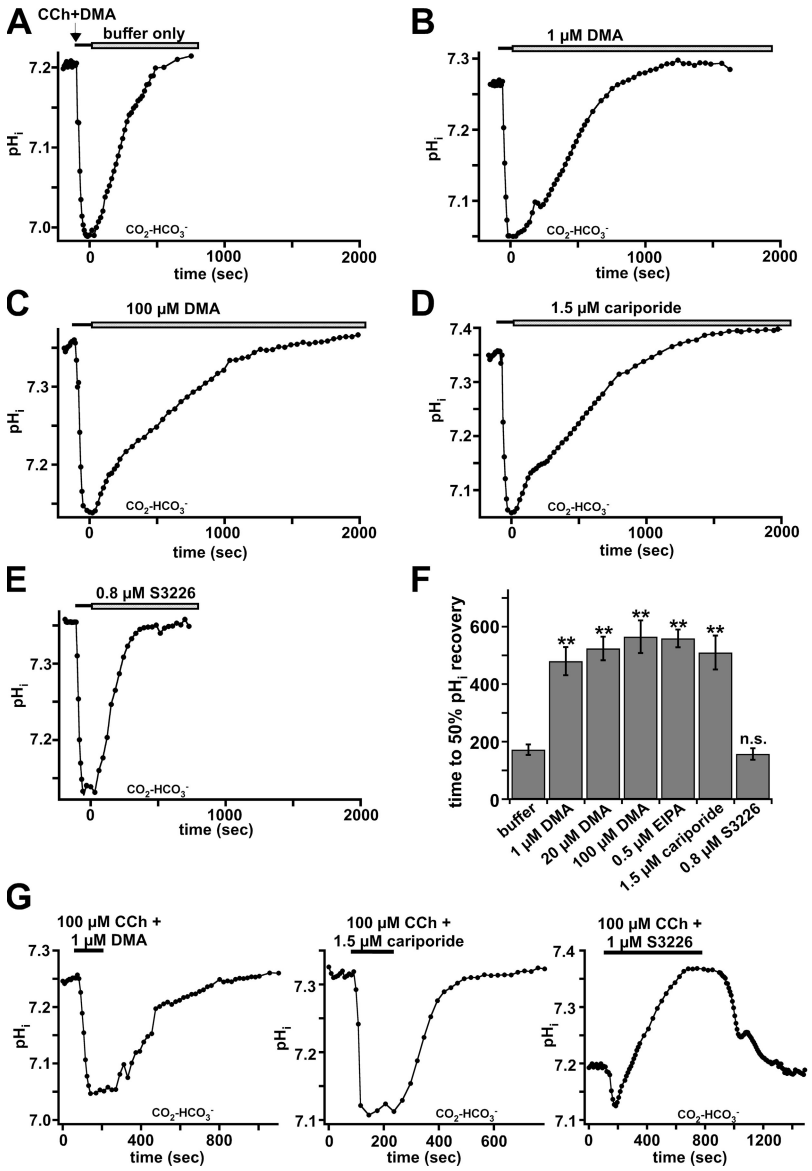

Figure 9. The NHE1 isoform is the major alkalinizing mechanism during CCh stimulation. (A–E) Representative experiments showing pH_i recovery (alkalinization) following acidification by 100 μM CCh stimulation in the presence of 30 μM DMA (~90 s; solid black bar) and subsequent removal of CCh and exposure to buffer only (A), 1 μM DMA (B), 30 μM DMA (not depicted), 100 μM DMA (C), 0.5 μM EIPA (not depicted), 1.5 μM cariporide (D), or 0.8 μM S3226 (E; open bars). Scales of x axes are identical, with the time of CCh removal set as $t = 0$ to facilitate comparisons among experiments. All experiments performed in presence of CO_2–HCO_3^-. (F) Summary from replicate experiments as shown above. Low concentrations of DMA and EIPA (1 μM and 0.5 μM, respectively) and the NHE1 inhibitor cariporide inhibited alkalinization similarly to a high concentration of DMA (100 μM), whereas the NHE3 inhibitor S3226 had no effect. Asterisks represent significance compared with buffer only. (G) Representative experiments of serous cells stimulated with 100 μM CCh in the presence of either 1 μM DMA (left trace), 1.5 μM cariporide (middle), or 1 μM S3226 (right). Cells stimulated in presence of DMA or cariporide exhibited enhanced prolonged acidification, while cells exposed to S3226 showed only transient acidification.

this alkalinization could serve as a mechanism for sustaining HCO_3^- secretion, we used a combination of targeted gene expression profiling, pharmacology, and immunocytochemistry.

The mRNA transcript expression of various known NHE isoforms was evaluated using single-cell aRNA amplification (Van Gelder et al., 1990; for review see Eberwine, 2001) followed by reverse transcription (rt)-PCR using NHE transcript-specific primers (listed in Table II). Single small homogenous serous acini (three to four cells; as described in Materials and methods) were isolated and subject to aRNA amplification followed by rtPCR using NHE isoform-specific primers. As controls, TRIzol-extracted RNA from brain, kidney, and salivary (parotid) gland was also used, as well as RNA amplified from small parotid acini using the aRNA method. NHE1 mRNA was detected in all samples used in these studies, including aRNA amplified from small submucosal gland serous and parotid acini (Fig. 8 A). Surprisingly, NHE2 and NHE3 transcripts were detected in RNA amplified from serous acinar cells and intact nasal turbinate tissue (Fig. 8, B and C). Neither NHE2 nor NHE3 was detected in RNA amplified from parotid acini (Fig. 8, B and C), but both transcripts were detected in RNA isolated from intact parotid gland (Fig. 8, B and C), in agreement with their expression in salivary gland ducts (Robertson et al., 1997; Park et al., 1999). As expected, NHE2 and NHE3 transcripts were detected in RNA isolated from kidney (unpublished data).

The physiological roles and expression patterns of the remaining isoforms are much less well studied. NHE4, shown to be expressed in the basolateral membranes of secretory and possibly absorptive epithelia (for review see Zachos et al., 2005), was detected in all RNA samples examined (including RNA from serous acinar cells and parotid acinar cells; Fig. 8 D). NHE5,

expressed mainly in brain ((Baird et al., 1999; for review see Orlowski and Grinstein, 2004), but also in spleen, skeletal muscle (Klanke et al., 1995), and sperm (Wang et al., 2003), was not detected in any of the samples tested (including submucosal gland acinar cells) except for brain RNA (Fig. 8 E). NHE6, NHE7, NHE8, and NHE9, believed to be ubiquitous and primarily intracellular (Nakamura et al., 2005), although NHE8 may also be apically expressed in renal cortex and/or medulla (Goyal et al., 2003, 2005; Becker et al., 2007; Kang'ethe et al., 2007; Zhang et al., 2007), were detected in RNA samples isolated from nasal, parotid, and kidney tissue, as well as serous acinar cells and parotid acinar cells (Figs. 8, F–I). Neither the sperm-specific NHE isoform termed mspermNHE (Wang et al., 2003) nor the osteoclast-specific NHE10 (Lee et al., 2008) were examined here.

These gene expression data suggest that transcripts for all of the well-characterized plasma membrane isoforms thought to be involved in epithelial ion/fluid secretion and absorption (NHE1–4) were detected in serous acinar cells, in contrast to the parotid acinar cells, where only NHE1 and NHE4 were detected. The variety of plasma membrane NHEs expressed in serous cells dictated that other methods were needed to determine which of these isoform(s) was/were required for the alkalinization observed during CCh stimulation.

The NHE1 Isoform Predominantly Contributes to Alkalinization during CCh Stimulation and during pH_i Recovery from CCh/DMA-induced Acidification

To elucidate the contributions of different NHE isoforms to agonist-induced alkalinization in submucosal gland serous acinar cells, several NHE inhibitors were used to construct a pharmacological profile of the observed alkalinization mechanism. As described above, stimulation with 100 μM CCh in the presence of 30 μM DMA led to an enhanced and prolonged acidification of ∼0.2 pH units. To test the effects of NHE inhibitors on pH_i recovery following this agonist-induced acidification, acinar cells were acidified by stimulation for ∼90 s with CCh in the presence of 30 μM DMA (as shown in Fig. 9, A–E, solid black bars), followed by removal of CCh and exposure of the cells to different concentrations of DMA or other NHE inhibitors (Fig. 9, A–E, open bars). Upon removal of both CCh and DMA ("buffer only" conditions), pH_i rapidly alkalinized to resting levels (time for recovery to 50% resting pH_i = 172 ± 17 s, n = 7; Fig. 9 A). However, when CCh was removed and cells were exposed to a low concentration of DMA (1 μM; Fig. 9, B and F), pH_i recovery was slowed by >2.5-fold. The time to 50% pH_i recovery in the presence of 1 μM DMA was 480 ± 49 s (n = 4; $P < 0.01$ compared with buffer only). The time for the return to 50% of resting pH_i in the presence of 30 μM DMA (524 ± 41 s; n = 7; Fig. 9 F) was also slower than the recovery observed in the presence of buffer alone ($P < 0.01$), but not enhanced (n.s.) beyond that observed in the presence of 1 μM DMA. A higher concentration of DMA (100 μM; Fig. 9, C and F) also increased the time to 50% pH_i recovery (565 ± 57 s, n = 4) compared with buffer alone ($P < 0.01$). However, the inhibition observed with 100 μM DMA was not increased beyond that observed with 30 μM DMA. These data are summarized in Fig. 9 F, and demonstrate that 1 μM DMA is a near-saturating concentration. Reported IC_{50} values (in μM) of DMA for NHE1, 2, and 3 are ∼0.023, 0.25, and 14, respectively (for review see Masereel et al., 2003). The lack of enhanced inhibition with [DMA] > 1 μM suggests that DMA-sensitive alkalinization is mediated by NHE1 and/or 2, typically classified as the "amiloride-sensitive" isoforms (for reviews see Masereel et al., 2003; Zachos et al., 2005). In agreement, a low concentration of another amiloride derivative, 5-(*N*-ethyl-*N*-isopropyl)amiloride (EIPA; 0.5 μM) also slowed pH_i recovery (trace not depicted, summarized in Fig. 9 F; 559 ± 31 s to 50% pH_i recovery, n = 5) compared with buffer only ($P < 0.01$). The inhibition of pH_i recovery with 0.5 μM EIPA was nearly identical to the inhibition observed with 30 μM DMA (n.s.). EIPA has IC_{50} values (in μM) of 0.01, 0.08, 2.4, and 2.5–10 for NHEs 1, 2, 3, and 4, respectively (Chambrey et al., 1997, 2001; Masereel et al., 2003). The strong inhibition observed with 1 μM DMA and 0.5 μM EIPA suggests that the DMA-sensitive component of the observed alkalinization is mainly due to the contributions of NHE1 and/or NHE2.

To further confirm the identity of the isoform(s) involved, we used the benzoylguanidine inhibitor cariporide (HOE 642), a strongly potent and selective NHE1 inhibitor. Previously reported IC_{50} values for cariporide are (in μM) ∼0.03 for NHE1, 4.3 for NHE2, >100 for NHE3 (Masereel et al., 2003), and >500 for NHE4 (Chambrey et al., 2001). A low dose of cariporide (1.5 μM) strongly inhibited pH_i recovery after CCh + DMA-induced acidification (Fig. 9, D and F; time to recovery to 50% pH_i = 511 ± 59 s, n = 7; $P < 0.01$ compared with buffer only). This was not different than the inhibition observed with 30 μM DMA (n.s.). In marked contrast, a low dose (0.8 μM) of the specific NHE3 inhibitor S3226 showed no inhibition of pH_i recovery after CCh + DMA-induced acidification (Fig. 9, E and F; time to return to 50% resting pH_i = 157 ± 20 s, n = 5). The IC_{50} value for S3226 is 0.02 μM for NHE3, compared with 3.6 μM for NHE1 and ∼80 μM for NHE2 (Schwark et al., 1998). Taken together, these data suggest that NHE1 is the primary NHE isoform contributing to pH_i recovery after CCh + 30 μM DMA–induced acidification.

In a separate experimental protocol, serous acinar cells were stimulated with 100 μM CCh in the presence of a low dose of DMA (1 μM), cariporide (1.5 μM), or S3226 (1 μM). In the presence of DMA or cariporide, a sustained and enhanced acidification was observed (Fig. 9 G, first and second panels). The CCh-induced acidification was 0.20 ± 0.03 U with 1 μM DMA (n = 3)

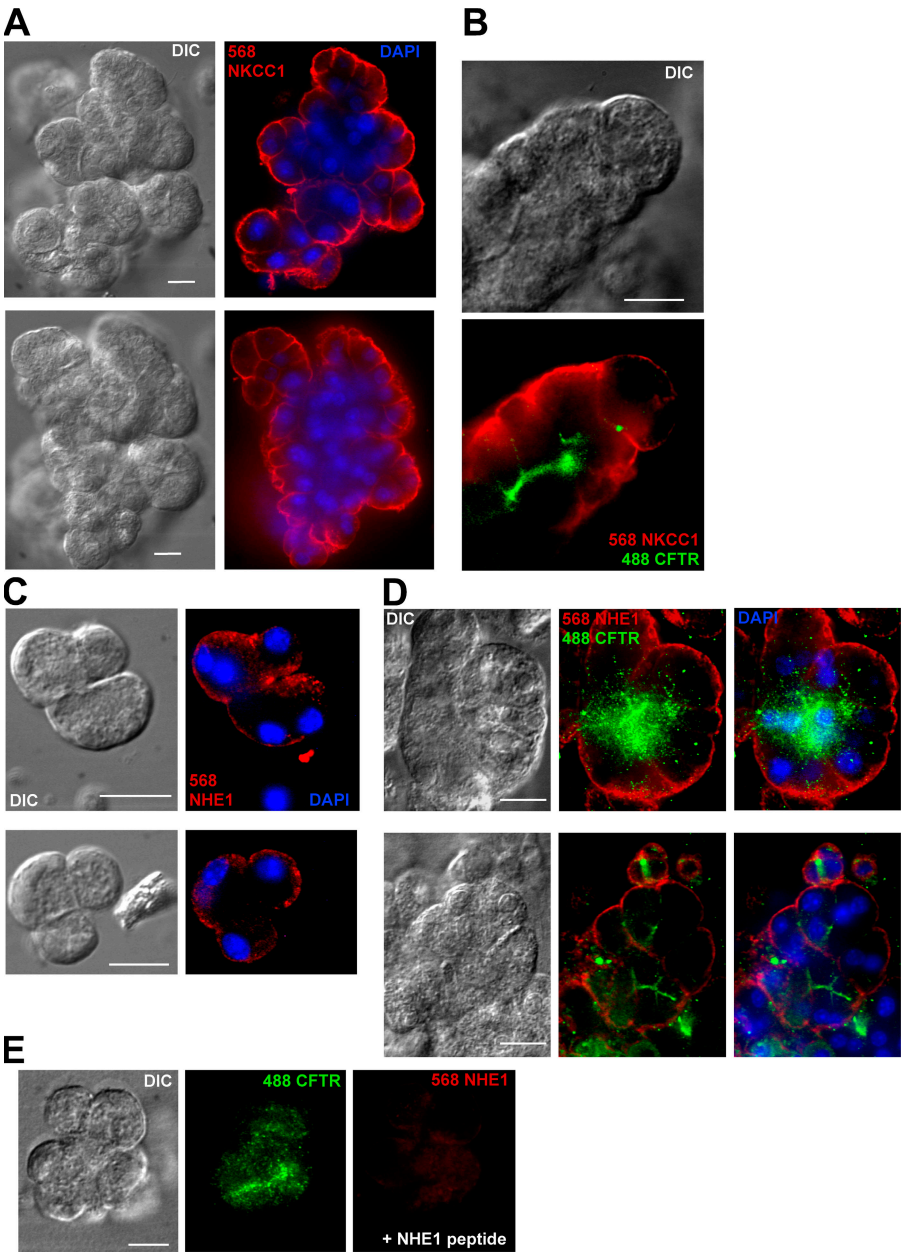

Figure 10. Confocal immunofluorescence microscopy indicates that NHE1 localizes to the basolateral membrane of serous acinar cells and acini. (A) Isolated, fixed serous acini exhibited NKCC1 immunofluorescence localized to the basolateral membranes. Top and bottom panels represent two separate focal planes imaged through same acinus. (B) Basolateral NKCC1 immunofluorescence did not overlap with CFTR, shown previously to be an apical serous cell marker. (C) NHE1 immunostaining revealed basolateral immunofluorescence pattern similar to that for NKCC1. (D) NHE1 immunofluorescence did not overlap with CFTR immunofluorescence. (E) Preincubation of NHE1 antibody with antigenic peptide reduced NHE1 immunofluorescence. Micrographs in E taken with identical system settings (filters, camera gain, exposure time, laser power) as used for images in D. Scale bar in each micrograph represents 10 μm.

and 0.21 ± 0.03 U with 1.5 μM cariporide ($n = 4$). This CCh-induced acidification was increased compared with that observed during stimulation with CCh alone ($P < 0.01$) but was identical to that observed during CCh stimulation in the presence of 30 μM DMA (n.s.). However, 100 μM CCh in the presence of 1 μM S3226 (Fig. 9 G, third panel) caused only a transient acidification (0.05 ± 0.01 units; $n = 8$) that was not different from that observed during stimulation with CCh alone (n.s.) but less than the acidification observed during CCh stimulation in the presence of 1 μM DMA ($P < 0.01$) or 1.5 μM cariporide ($P < 0.01$). Taken together, these data suggest that NHE1 is the major NHE isoform that contributes to alkalinization of pH_i during conditions of CCh stimulation.

NHE1 Is Expressed on the Basolateral Membrane of Serous Acinar Cells

For the observed CCh-induced NHE1 activity to indeed serve as a mechanism for sustaining HCO_3^- secretion, NHE1 expression must be localized to the basolateral membrane of the serous epithelium. If NHE1 were instead localized to the apical membrane, HCO_3^- secretion would be neutralized by the parallel efflux of H^+ into the acinar lumen. The localization of NHE1 was investigated by confocal immunofluorescence microscopy of isolated fixed acini and acinar cells using a polyclonal antibody against NHE1. As a control, immunostaining was also performed using a polyclonal antibody to NKCC1, a well-characterized protein expressed on the basolateral membrane of secretory epithelia (for reviews

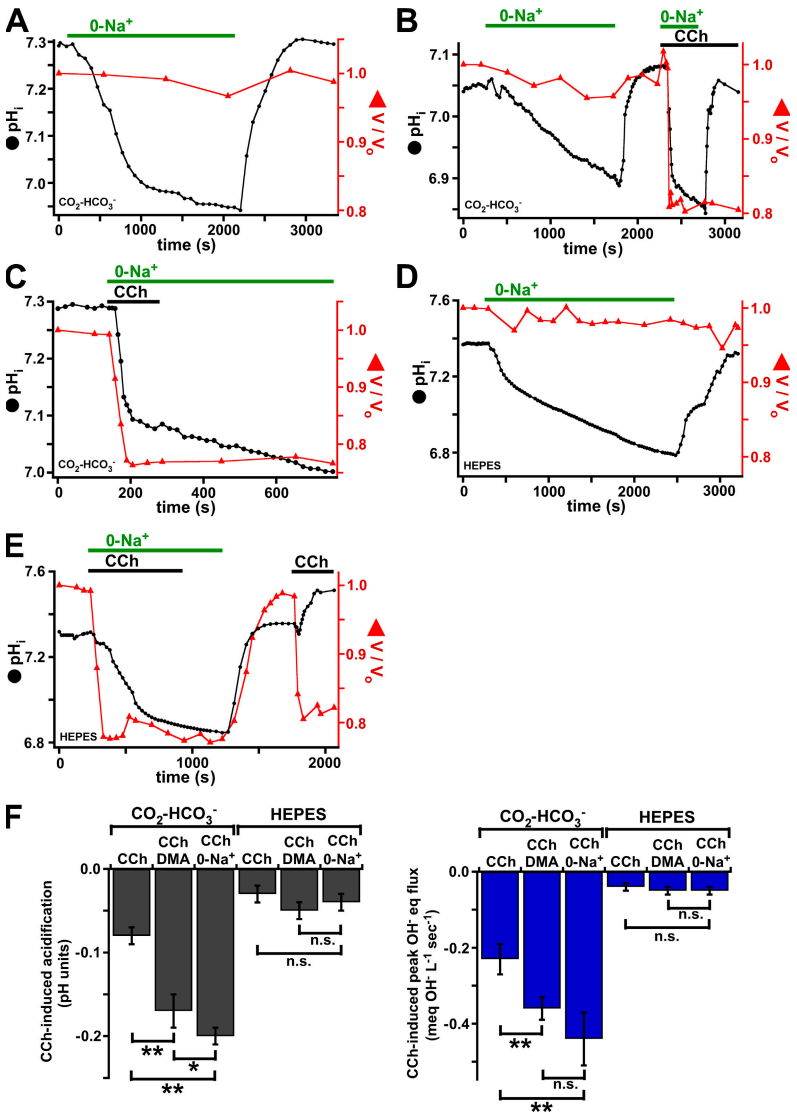

Figure 11. Removal of Na^+_o enhances CCh-induced acidification and completely blocks pH_i recovery. Representative experiments illustrating dependence of serous cell pH_i on Na^+_o. (A) Removal of Na^+_o (0 Na^+) in CO_2–HCO_3^- (Solution C) caused slow acidification. Cells recovered to near resting pH_i upon reintroduction of Na^+_o. (B) Stimulation of acinar cells with 100 µM CCh in 0 Na^+ solution elicited enhanced acidification compared with 0 Na^+ alone or CCh alone. (C) Cells stimulated with CCh in 0 Na^+ exhibited slow, progressive acidification following immediate rapid CCh-induced acidification, and lacked pH_i or volume recovery upon removal of CCh. (D) Removal of Na^+_o in HEPES buffer (Solution D) also caused prolonged acidification, with realkalinization upon reintroduction of Na^+_o. (E) CCh stimulation in HEPES-buffered 0 Na^+ solution enhanced CCh-induced acidification, but to a smaller extent than observed in CO_2–HCO_3^- buffer. (F) Summary of CCh-induced acidification (left) and peak OH^- eq fluxes (right) in Na^+-containing and 0 Na^+ CO_2–HCO_3^- and HEPES buffers.

see Gerelsaikhan and Turner, 2000; Haas and Forbush, 2000). Strong NKCC1 immunofluorescence was detected along apparent basal and lateral membranes of serous acini (Fig. 10 A), in agreement with functional and genetic evidence of NKCC1 expression in murine serous acinar cells (Lee et al., 2007), and functional data suggesting NKCC contributes to CCh-induced fluid secretion from intact murine submucosal glands (Ianowski et al., 2007). NKCC1 immunofluorescence did not overlap with immunofluorescence for CFTR (Fig. 10 B), previously shown to be expressed apically in serous acini (Engelhardt et al., 1992; Jacquot et al., 1993; Lee et al., 2007). The distinct patterns of NKCC1 and CFTR immunostaining support the basolateral localization of the NKCC1 immunofluorescence pattern. A similar basolateral immunofluorescence pattern was observed for NHE1 (Fig. 10 C). NHE1 immunofluorescence also did not overlap with CFTR immunofluorescence (Fig. 10 D). When NHE1 antibody was preincubated with excess antigenic peptide, NHE1 immunofluorescence was significantly reduced while CFTR immunofluorescence was unaffected (Fig. 10 E), supporting the specificity of the NHE1 immunostaining. These data indicate that that the basolateral membrane is the major site of NKCC1 and NHE1 expression in serous acinar cells, consistent with the hypothesis that NHE1 plays a crucial role in HCO_3^- secretion during CCh stimulation.

Removal of Extracellular Na^+ Leads to a Slow Prolonged Acidification and Completely Inhibits pH_i Recovery after CCh-induced Acidification, but Does Not Significantly Enhance the Initial CCh-induced OH^- Eq Flux

The above data suggest that NHE1 is the main NHE isoform contributing to alkalinization during CCh-stimulated fluid secretion and during pH_i recovery from CCh-induced acidification, and suggest that NHE1 localization would permit it to function in maintaining HCO_3^- secretion. However, other pH_i regulatory mechanisms exist in serous acinar cells, as evidenced by the ability of cells to alkalinize, albeit very slowly, in the presence of

100 μM DMA. It is possible that Na^+-linked DMA-insensitive transporters, for example Na^+–HCO_3^- cotransporters (NBCs), may be involved. The Na^+ dependence of both resting pH_i regulation and pH_i recovery after CCh-induced acidification was evaluated using 0 Na^+ solutions (Na^+ isosmotically replaced by $NMDG^+$). In CO_2–HCO_3^--buffered conditions, removal of Na^+ from the extracellular medium led to a continuous acidification (Fig. 11 A), suggesting that Na^+ is required for regulation of resting pH_i. The acidification was slow (0.01 ± 0.003 pH unit·min^{-1} during the first 10 min of observation), with a maximal net OH^- eq flux of −0.04 ± 0.01 meq OH^-·$liter^{-1}$·min^{-1} (n = 6). CCh stimulation in 0 Na^+ CO_2–HCO_3^- buffer (Fig. 11, B and C) caused an immediate fast drop in pH_i of 0.20 ± 0.01 U (n = 8). This was ∼2.5-fold larger than the acidification observed with CCh stimulation in normal Na^+-containing CO_2–HCO_3^- buffer ($P < 0.01$) and also slightly larger than that observed with CCh stimulation in Na^+-containing CO_2–HCO_3^- buffer in the presence of 30 μM DMA ($P < 0.05$). The peak CCh-induced OH^- eq flux in Na^+-free CO_2–HCO_3^- buffer was −0.44 ± 0.07 meq OH^-·$liter^{-1}$·s^{-1} (n = 8). This value was approximately twofold larger than that observed with CCh stimulation in Na^+-containing CO_2–HCO_3^- buffer ($P < 0.01$) but nearly identical to that observed during CCh stimulation in Na^+-containing CO_2–HCO_3^- buffer in the presence of 30 μM DMA (n.s.). CCh-induced acidification and OH^- eq flux values are summarized in Fig. 11 F.

The fact that CCh-induced OH^- eq efflux and acidification in 0 Na^+ solution were only slightly enhanced compared with those observed in Na^+-containing solution with saturating [DMA] strongly suggests that NHE1 is the major alkalinizing mechanism activated during CCh stimulation. However, the slow alkalinization mechanisms observed in cells stimulated with CCh in the presence of DMA were absent in cells stimulated with CCh in 0 Na^+ buffer, as cells continued to acidify after the initial CCh-induced drop (Fig. 11 C) regardless of whether CCh was removed. The complete lack of pH_i recovery in 0 Na^+ solution suggests that the DMA-insensitive pH_i recovery mechanism(s) observed in the cells are strongly dependent upon extracellular Na^+. In contrast, 0 Na^+ conditions did not affect CCh-induced cell shrinkage (23 ± 1%) or maximal Cl^- flux rate (−1.7 ± 0.2 meq·Cl^-·$liter^{-1}$·s^{-1}; n = 8) compared with CCh stimulation in Na^+-containing buffer (n.s.). However, cell swelling upon removal of CCh was completely blocked in 0 Na^+ conditions (Fig. 11 C), likely due to total inhibition of NKCC1.

In the absence of CO_2–HCO_3^-, removal of Na^+ (0 Na^+ Solution D; Fig. 11 D) also caused pH_i to fall (−0.03 ± 0.01 pH unit·min^{-1} during the first 10 min of observation), faster than that observed under 0 Na^+ conditions in the presence of CO_2–HCO_3^- ($P < 0.05$). However, this apparent increased rate was due to the reduced buffering capacity of cells lacking β_{HCO3-}, as the peak net OH^- eq flux (−0.05 ± 0.02 meq OH^-·$liter^{-1}$·min^{-1}; n = 7) was not increased beyond that observed in 0 Na^+ CO_2–HCO_3^- buffer (n.s.). The initial CCh-induced acidification (0.04 ± 0.01 pH units) and OH^- eq flux values (−0.05 ± 0.01 meq OH^-·$liter^{-1}$·min^{-1}; n = 5) in 0 Na^+ HEPES-buffered solution were identical to those observed during CCh stimulation in Na^+-containing HEPES buffer (n.s.). However, the CCh-induced acidification and OH^- eq flux values in 0 Na^+ HEPES buffer were only ∼25% and ∼12%, respectively, of those observed in 0 Na^+ CO_2–HCO_3^- buffer ($P < 0.01$ for both; Fig. 11, E and F). Nevertheless, as observed in CO_2–HCO_3^- buffer, cells exhibited no ability to recover either pH_i or cell volume under Na^+-free CO_2–HCO_3^--free conditions (Fig. 11 E), as pH_i continued to acidify for >30 min of observation. Taken together, these data suggest that DMA-insensitive Na^+-dependent pH_i regulatory mechanisms are involved in maintenance of resting pH_i and full recovery after agonist-induced acidification.

DISCUSSION

Serous Acinar Cells Secrete HCO_3^- in Response to Muscarinic Stimulation

Exocrine gland fluid secretion is mediated by a complex set of ion channels and transporters acting in concert and subject to intricate feedback and regulatory mechanisms (for review see Melvin et al., 2005). The generalized model of epithelial fluid secretion dictates that secondarily active basolateral transport (coupled to the Na^+ gradient and membrane potential generated by the Na^+/K^+ ATPase) leads to accumulation of anions (Cl^-, HCO_3^-) inside the secretory cell at concentrations above their electrochemical equilibrium. During secretion, these anions can exit across the apical membrane, with basolateral K^+ channels allowing for efflux of K^+ and maintenance of electroneutrality. The resulting negative transepithelial potential draws Na^+ across the epithelium, likely through a paracellular pathway, and osmotically obliged water follows the movement of the Na^+ and Cl^- ions. We previously examined the mechanisms of fluid secretion in airway submucosal gland serous acinar cells from murine nasal tissues, by imaging agonist-induced cell volume changes to track changes in cell solute content, along with fluorescence microscopy of ion indicator dyes (Lee et al., 2007). Serous cells stimulated with CCh shrank by ∼20% in response to a muscarinic-induced increase in $[Ca^{2+}]_i$ and stimulation of Ca^{2+}-activated membrane permeabilities. Cell shrinkage was caused by efflux of >60% of cell Cl^- content associated with activation of Cl^- secretion. Sustained Cl^- secretion required the activity of the NKCC1 cotransporter, with no apparent involvement of coupled Na^+/H^+ and Cl^-/HCO_3^- exchangers.

In this study, the capacity of acinar cells to secrete HCO_3^- was evaluated. We performed quantitative measurements of pH_i at rest and during cholinergic stimulation. Because changes in cell volume provide information regarding the fluid secretory state of the cells, cell volume was measured simultaneously with pH_i. Our results indicate that cholinergic stimulation of fluid secretion is associated with activation of two major mechanisms that acidify and alkalinize the cells, respectively, that together mediate HCO_3^- secretion. Several pieces of evidence suggest that the initial rapid acidification was caused predominately by HCO_3^- efflux. First, the magnitude of the acidification was greatly enhanced by the presence of CO_2–HCO_3^- in the medium. This was particularly evident when activation-induced alkalinization mechanisms (Na^+/H^+ exchange) were inhibited. Importantly, elimination of the electrochemical driving force for conductive HCO_3^- efflux (clamping $V_m = E_{HCO3-}$) by manipulation of the concentrations of K^+ and Cl^-, the two major ions that determine membrane potential in acinar cells, nearly completely eliminated the acidification. This result suggests that the acidification is mediated by HCO_3^- efflux, and furthermore that the efflux mechanism is conductive.

The Nature of the HCO_3^- Efflux Pathway

The kinetics of the agonist-induced acidification closely followed the kinetics of Cl^- efflux, as the time course of the initial cell shrinkage and acidification were similar, and the maximum Cl^- and OH^- eq efflux rates coincided temporally. These results suggest that the HCO_3^- conductance pathway might be the same as that for Cl^-. We found that neither Cl^- nor HCO_3^- efflux in response to CCh was dependent on CFTR, as they were unaffected in cells isolated from *cftr*$^{tm1Unc-/-}$ mice (this study and Lee et al., 2007). This result was not surprising considering that CCh-evoked secretion rates measured from murine *cftr*$^{tm1Unc-/-}$ submucosal glands are identical to rates observed in Wt glands (Ianowski et al., 2007). To test the involvement of other Cl^- channels, we examined the effects of the nonspecific Cl^- channel inhibitor NFA, previously shown to inhibit CCh-evoked fluid secretion from intact murine submucosal glands (Ianowski et al., 2007).We found that NFA inhibited CCh-induced Cl^- efflux from isolated serous cells, strongly suggesting that non-CFTR Cl^- channels account for cholinergic-induced Cl^- secretion in murine serous acinar cells. Importantly, NFA also nearly completely blocked the cholinergic-induced acidification. The temporal coincidence of the Cl^- efflux and HCO_3^--dependent acidification and their similar pharmacological sensitivities together suggest that HCO_3^- efflux is mediated by the same pathway that mediates Ca^{2+}-activated Cl^- efflux.

An important caveat to use of isolated cells is lack of information regarding the apical vs. basolateral polarization of the ion transport mechanisms examined, in particular the Cl^- and HCO_3^- efflux pathways experimentally examined here. It is possible that a component of the Cl^- and HCO_3^- efflux we observed is mediated by basolaterally localized Cl^- channels. However, the accepted model of exocrine gland Cl^-/fluid secretion (for review see Melvin et al., 2005), supported by data from intact tissue preparations, is that the majority of secretagogue-regulated anion conductances are localized to the apical membrane, as basolaterally localized anion channels would "short circuit" the vectoral anion transport that drives fluid secretion. Cultured primary tracheal ciliated epithelial cells possess basolateral Cl^- channels (Fischer et al., 2007), but these likely play a role in fluid absorptive properties of the surface epithelium. Basolateral Cl^- channel expression has not been directly demonstrated for serous or other submucosal gland cell types. The simplest and most likely interpretation of our results is that the majority of secretagogue-stimulated Cl^- efflux we observed reflects CCh-evoked Cl^- secretion through the secretory Cl^- channel(s), as concluded in studies in other dispersed secretory acinar cells (for review see Melvin et al., 2005). This interpretation is further strongly supported by the similar NFA sensitivity of both CCh-induced acinar cell Cl^- efflux and intact gland fluid secretion.

Assuming that almost all of the CCh-stimulated OH^- eq efflux represents HCO_3^- efflux (as the ion substitution data suggest), and that the efflux pathway for Cl^- and HCO_3^- is the same (as the NFA data suggest), then the values determined for HCO_3^- and Cl^- fluxes can be used to provide a rough estimate of the Cl^-:HCO_3^- conductance ratio of the anion efflux pathway. The flux (J) is equal to the product of the conductance (G) and the driving force (DF), or $J = G \cdot DF$, and $J_{Cl-}/J_{HCO3-} = (G_{Cl-} \cdot DF_{Cl-})/(G_{HCO3-} \cdot DF_{HCO3-})$.

The driving force is equal to the sum of the electrical and chemical driving force. While the membrane potential in these experiments is unknown, the electrical driving force for HCO_3^- and Cl^- efflux is the same since both are monovalent anions, allowing the electrical term to be ignored and requiring only a comparison of the concentration ratios. Thus, $J_{Cl-}/J_{HCO3-} = (G_{Cl-} \cdot ([Cl^-]_i/[Cl^-]_o)) / (G_{HCO3-} \cdot ([HCO_3^-]_i/[HCO_3^-]_o))$. At resting $pH_i = 7.2$ and $pH_o = 7.4$, $[HCO_3^-]_i/[HCO_3^-]_o = 16$ mM/25 mM = 0.64. Assuming resting $[Cl^-]_i = 65$ mM, $[Cl^-]_i/[Cl^-]_o = 65$ mM/135 mM = 0.48. Using the efflux rates determined during stimulation with CCh in the presence of 30 μM DMA, -1.7 meq·liter^{-1}·s^{-1} and -0.36 meq·liter^{-1}·s^{-1} for Cl^- and HCO_3^-, respectively, $G_{Cl-}/G_{HCO3-} = (-1.7 \cdot 0.64)/(-0.36 \cdot 0.48) = 1.1/0.17 = 6.5$.

This estimation gives a Cl^-/HCO_3^- conductance of ~6.5, similar to Cl^-/HCO_3^- conductance values (~5) previously reported for Ca^{2+}-activated Cl^- channels (Qu and Hartzell, 2000; for review see Hartzell et al., 2005). The ratio of fluxes and their mutual NFA sensitivity suggest that a Ca^{2+}-activated Cl^- channel serves a dual role in serous acinar cells as the primary cholinergic-activated

secretion pathway for both Cl^- and HCO_3^-. The identity of this Ca^{2+}-activated Cl^- channel(s) in the airway is/are yet to be determined, as is the expression of potential candidate channel proteins (bestrophins, etc.) in submucosal gland serous cells.

Taken together, our data suggest that CCh induces HCO_3^- secretion from airway gland serous cells. Previous work has demonstrated that cholinergic-induced fluid secretion by intact murine and porcine glands is significantly blocked by removal of CO_2–HCO_3^- from the extracellular medium (Inglis et al., 1997a, 1998; Ballard et al., 1999; Joo et al., 2001a,b, 2002b; Ianowski et al., 2007). While these data suggest that HCO_3^- plays an important role in secretion, they are difficult to interpret, since inhibition could be caused by either a primary defect of serous cell secretion or defective modification of secreted fluid elsewhere in the gland. Our results suggest that CCh-evoked murine serous cell fluid secretion does not depend strongly on the presence of HCO_3^-, as we observed little effect of removal of HCO_3^- on CCh-evoked Cl^- dynamics, and our previous data showed that basolateral Cl^- accumulation is primarily dependent on NKCC1 and not NHE/AE.

We previously concluded that serous cell volume changes in response to CCh are due almost entirely due to a loss of KCl content (Lee et al., 2007). Our results here indicate that a portion also reflects loss of $KHCO_3$. However, the HCO_3^- content lost is small, as $[HCO_3^-]_i$ would be expected to fall at most from ~16 mM (at pH_i = 7.2) to ~12 mM at (pH_i = 7.0; the approximate pH_i after stimulation with 100 μM CCh + 30 μM DMA). Taking into account the change in cell volume (V/V_o from 1 to ~0.8), the cells would have lost at most (16 meq·liter^{-1} × 1) − (12 meq·liter^{-1} × 0.8) = ~6.4 meq·liter^{-1} of HCO_3^- content. This is approximately sevenfold less than the 44 meq·liter^{-1} of Cl^- content lost during CCh stimulation (Lee et al., 2007). In reality, the cells lose even less, because activation of NHE1 restores lost HCO_3^- content by raising pH_i and enabling CO_2 to be continuously hydrated to form HCO_3^-.

Optical measurements of conductive Cl^- and HCO_3^- effluxes are not as direct as electrophysiological characterization of HCO_3^- and Cl^- currents. However, we have found patch clamp electrophysiology of murine serous acinar cells to be challenging because seal formation is rare, likely due to the presence of connective tissue that has been difficult to remove without overdigesting and killing the cells. Alternately, our optical approaches have enabled study of these pathways in intact cells with intact signal transduction mechanisms, and they have enabled us to elucidate the contributions (or lack thereof) of electroneutral processes such as Na^+/H^+ or Cl^-/HCO_3^- exchange.

NHE1 Sustains HCO_3^- Secretion

Our data suggest that NHE1 activity in airway serous acinar cells is strongly up-regulated in response to CCh stimulation. Aside from the ubiquitous role of NHE1 in pH_i homeostasis in almost all cell types, NHE1 has been coopted by secretory epithelia to serve a variety of functions. Basolaterally expressed NHE1 functions in combination with Cl^-/HCO_3^- exchangers to facilitate Cl^- accumulation and sustain transepithelial Cl^- secretion in the parotid gland (Robertson and Foskett, 1994; for review see Melvin et al., 2005). However, in the murine airway submucosal gland serous cells studied here, the primary function of NHE1 appears to be to raise pH_i during stimulated fluid secretion. By keeping pH_i elevated during agonist-activated HCO_3^- efflux, basolateral NHE1 can act as a major mechanism to sustain HCO_3^- secretion.

Ballard and colleagues demonstrated that DMA inhibited >50% of bumetanide-insensitive liquid secretion and nearly 50% of HCO_3^- secretion by excised porcine bronchi (Trout et al., 1998a, 2001) and that DMA affected the composition of fluid and mucus secreted from intact porcine submucosal glands (Inglis et al., 1997a, 1998; Trout et al., 1998b). Our results here suggest that those observations could be accounted for, at least in part, by DMA inhibition of NHE1-dependent sustained HCO_3^- secretion from submucosal gland serous acini. In the future, the methods described here will be translated to isolated porcine serous cells to test this hypothesis.

The molecular mechanisms of cholinergic activation of NHE1 in murine airway serous acinar cells is unclear. It is unlikely that the initial HCO_3^- efflux is a signal, since agonist-induced alkalinization was observed in the absence of a strong initial acidification when the cells were stimulated in CO_2–HCO_3^--free conditions. Muscarinic activation of NHE1 in salivary acinar cells is mediated by increased $[Ca^{2+}]_i$, independent of calmodulin and PKC (Manganel and Turner, 1989, 1990, 1991; Okada et al., 1991; Robertson et al., 1997), whereas recombinant NHE1 requires calmodulin and/or PKC for agonist-induced activation (for reviews see Putney et al., 2002; Malo and Fliegel, 2006). Whether these pathways are required for NHE1 activation in airway serous acinar cells remains to be determined.

Our data support the existence of other Na^+-dependent, but DMA-insensitive, mechanisms in serous cells that play an important role in regulating resting pH_i, in agreement with conclusions reached in intact porcine submucosal glands (Hug and Bridges, 2001). The identity and role of other H^+ and/or HCO_3^--linked transporters, including NBC isoforms, remains to be elucidated.

Possible Importance of Serous Cell HCO_3^- Secretion for Normal and Pathogenic Airway Fluid Homeostasis

The secreted fluid product from intact submucosal glands has been consistently determined to be near or slightly less than neutral pH (Jayaraman et al., 2001; Joo et al., 2001a; Song et al., 2006). However, our results suggest that serous acinar cells secrete a primary alkaline fluid.

Unless serous cells possess unknown mechanisms to further modify rates or amounts of HCO_3^- secretion that have remained undetected in our experiments, these results suggest that fluid secreted by serous cells may be modified by other cell types during its transit to the airway surface epithelium. It is possible that an initial alkaline pH of the primary secreted fluid is important as it washes past mucous cells and hydrates released mucous granules. Modifications of the primary secreted fluid may be accomplished by ion transport mechanisms in mucous and/or collecting duct cells that are still unknown. The methods presented here could be adapted to study ion transport pathways in these cell types.

In the genetic disease CF, it has been speculated that lung disease may be due not only to a reduced quantity, but also to altered composition of the ASL. In particular, it has been speculated that HCO_3^- secretion and regulation of ASL pH may play an important role in CF pathology (for review see Quinton, 1999, 2001). It has been suggested that CF ASL may be acidic compared with normal ASL (for review see Coakley and Boucher, 2001), and that isolated intact submucosal glands from CF patients produce a hyperacidic product compared with control glands (Song et al., 2006), although the mechanisms involved are unknown. Our data suggest that serous acinar cells can support HCO_3^- secretion in response to cholinergic stimulation, likely through a Ca^{2+}-activated Cl^- channel. Because cholinergic-stimulated secretion in CF submucosal glands is intact, this supports the possibility that the Ca^{2+}-stimulated secretion pathway and/or alternative Cl^- channels may be important therapeutic targets for CF treatment if impairment of cAMP-activated HCO_3^- secretion from serous cells contributes to CF pathology. However, it still remains to be determined if serous acinar cells secrete HCO_3^- in response to cAMP agonists, and whether any cAMP-induced HCO_3^- secretion is altered in cells lacking functional CFTR. In the future, the optical techniques developed and outlined in this study will be used to examine the role of cAMP and CFTR in serous cell HCO_3^- secretion to begin to address whether this process is impaired in CF.

The authors wish to thank Dr. D.-O.D. Mak for assistance with analyses of flux data, Dr. R.J. Turner for antibody to NKCC1, Dr. J. Puenter (Sanofi-Aventis, Frankfurt, Germany) for gifts of cariporide and S3226, and Ms. R. Munden for excellent animal assistance.

R.J. Lee was supported by predoctoral fellowships from the National Science Foundation and the Cystic Fibrosis Foundation. J.M. Harlow was supported by RDP-R881 from the Cystic Fibrosis Foundation. This study was funded by grant FOSKET07G0 from the Cystic Fibrosis Foundation to J.K. Foskett.

Angus C. Nairn served as editor.

Submitted: 4 April 2008
Accepted: 27 May 2008

REFERENCES

Baird, N.R., J. Orlowski, E.Z. Szabo, H.C. Zaun, P.J. Schultheis, A.G. Menon, and G.E. Shull. 1999. Molecular cloning, genomic organization, and functional expression of Na^+/H^+ exchanger isoform 5 (NHE5) from human brain. *J. Biol. Chem.* 274:4377–4382.

Ballard, S.T., and S.K. Inglis. 2004. Liquid secretion properties of airway submucosal glands. *J. Physiol.* 556:1–10.

Ballard, S.T., and D. Spadafora. 2007. Fluid secretion by submucosal glands of the tracheobronchial airways. *Respir. Physiolo. Neurobiol.* 159:271–277.

Ballard, S.T., L. Trout, Z. Bebok, E.J. Sorscher, and A. Crews. 1999. CFTR involvement in chloride, bicarbonate, and liquid secretion by airway submucosal glands. *Am. J. Physiol.* 277:L694–L699.

Becker, A.M., J. Zhang, S. Goyal, V. Dwarakanath, P.S. Aronson, O.W. Moe, and M. Baum. 2007. Ontogeny of NHE8 in the rat proximal tubule. *Am. J. Physiol. Renal Physiol.* 293:F255–F261.

Boron, W.F. 2004. Regulation of intracellular pH. *Adv. Physiol. Educ.* 28:160–179.

Boron, W.F., and P. De Weer. 1976. Intracellular pH transients in squid giant axons caused by CO_2, NH_3, and metabolic inhibitors. *J. Gen. Physiol.* 67:91–112.

Brown, D.A., J.E. Melvin, and D.I. Yule. 2003. Critical role for NHE1 in intracellular pH regulation in pancreatic acinar cells. *Am. J. Physiol. Gastrointest. Liver Physiol.* 285:G804–G812.

Buckler, K.J., and R.D. Vaughan-Jones. 1990. Application of a new pH-sensitive fluoroprobe (carboxy-SNARF-1) for intracellular pH measurement in small, isolated cells. *Pflugers Arch.* 417:234–239.

Chambrey, R., J.M. Achard, and D.G. Warnock. 1997. Heterologous expression of rat NHE4: a highly amiloride-resistant Na^+/H^+ exchanger isoform. *Am. J. Physiol.* 272:C90–C98.

Chambrey, R., P.L. St John, D. Eladari, F. Quentin, D.G. Warnock, D.R. Abrahamson, R.A. Podevin, and M. Paillard. 2001. Localization and functional characterization of Na^+/H^+ exchanger isoform NHE4 in rat thick ascending limbs. *Am. J. Physiol. Renal Physiol.* 281:F707–F717.

Coakley, R.D., and R.C. Boucher. 2001. Regulation and functional significance of airway surface liquid pH. *JOP.* 2:294–300.

Eberwine, J. 2001. Single-cell molecular biology. *Nat. Neurosci.* 4(Suppl):1155–1156.

Engelhardt, J.F., J.R. Yankaskas, S.A. Ernst, Y. Yang, C.R. Marino, R.C. Boucher, J.A. Cohn, and J.M. Wilson. 1992. Submucosal glands are the predominant site of CFTR expression in the human bronchus. *Nat. Genet.* 2:240–248.

Evans, R.L., S.M. Bell, P.J. Schultheis, G.E. Shull, and J.E. Melvin. 1999. Targeted disruption of the Nhe1 gene prevents muscarinic agonist-induced up-regulation of Na^+/H^+ exchange in mouse parotid acinar cells. *J. Biol. Chem.* 274:29025–29030.

Fischer, H., B. Illek, W.E. Finkbeiner, and J.H. Widdicombe. 2007. Basolateral Cl channels in primary airway epithelial cultures. *Am. J. Physiol. Lung Cell. Mol. Physiol.* 292:L1432–L1443.

Foskett, J.K. 1988. Simultaneous Nomarski and fluorescence imaging during video microscopy of cells. *Am. J. Physiol.* 255:C566–C571.

Foskett, J.K. 1990a. $[Ca^{2+}]i$ modulation of Cl^- content controls cell volume in single salivary acinar cells during fluid secretion. *Am. J. Physiol.* 259:C998–C1004.

Foskett, J.K. 1990b. Optical studies of ion and water transport in single living cells. *In* Noninvasive Techniques in Cell Biology. J.K. Foskett and S. Grinstein, editors. Wiley-Liss, Inc., New York. 237–272.

Foskett, J.K. 1993. Optical imaging of ion transport in single living cells. *Comments Mol. Cell. Biophys.* 8:115–135.

Gerelsaikhan, T., and R.J. Turner. 2000. Membrane topology and function of the secretory Na^+-K^+-2Cl- cotransporter (NKCC1). *J. Korean Med. Sci.* 15(Suppl):S3–S4.

Goyal, S., G. Vanden Heuvel, and P.S. Aronson. 2003. Renal expression of novel Na^+/H^+ exchanger isoform NHE8. *Am. J. Physiol. Renal Physiol.* 284:F467–F473.

Goyal, S., S. Mentone, and P.S. Aronson. 2005. Immunolocalization of NHE8 in rat kidney. *Am. J. Physiol. Renal Physiol.* 288:F530–F538.

Grubb, B.R., and R.C. Boucher. 1999. Pathophysiology of gene-targeted mouse models for cystic fibrosis. *Physiol. Rev.* 79:S193–S214.

Haas, M., and B. Forbush III. 2000. The Na-K-Cl cotransporter of secretory epithelia. *Annu. Rev. Physiol.* 62:515–534.

Hartzell, C., I. Putzier, and J. Arreola. 2005. Calcium-activated chloride channels. *Annu. Rev. Physiol.* 67:719–758.

Huang, P., E. Gilmore, P. Kultgen, P. Barnes, S. Milgram, and M.J. Stutts. 2004. Local regulation of cystic fibrosis transmembrane regulator and epithelial sodium channel in airway epithelium. *Proc. Am. Thorac. Soc.* 1:33–37.

Hug, M.J., and R.J. Bridges. 2001. pH regulation and bicarbonate transport of isolated porcine submucosal glands. *JOP.* 2:274–279.

Ianowski, J.P., J.Y. Choi, J.J. Wine, and J.W. Hanrahan. 2007. Mucus secretion by single tracheal submucosal glands from normal and CFTR knock-out mice. *J. Physiol.* 580:301–314.

Inglis, S.K., M.R. Corboz, A.E. Taylor, and S.T. Ballard. 1997a. Effect of anion transport inhibition on mucus secretion by airway submucosal glands. *Am. J. Physiol.* 272:L372–L377.

Inglis, S.K., M.R. Corboz, A.E. Taylor, and S.T. Ballard. 1997b. In situ visualization of bronchial submucosal glands and their secretory response to acetylcholine. *Am. J. Physiol.* 272:L203–L210.

Inglis, S.K., M.R. Corboz, and S.T. Ballard. 1998. Effect of anion secretion inhibitors on mucin content of airway submucosal gland ducts. *Am. J. Physiol.* 274:L762–L766.

Jacquot, J., E. Puchelle, J. Hinnrasky, C. Fuchey, C. Bettinger, C. Spilmont, N. Bonnet, A. Dieterle, D. Dreyer, A. Pavirani, et al. 1993. Localization of the cystic fibrosis transmembrane conductance regulator in airway secretory glands. *Eur. Respir. J.* 6:169–176.

Jayaraman, S., N.S. Joo, B. Reitz, J.J. Wine, and A.S. Verkman. 2001. Submucosal gland secretions in airways from cystic fibrosis patients have normal $[Na^+]$ and pH but elevated viscosity. *Proc. Natl. Acad. Sci. USA.* 98:8119–8123.

Joo, N.S., M.E. Krouse, J.V. Wu, Y. Saenz, S. Jayaraman, A.S. Verkman, and J.J. Wine. 2001a. $HCO3^-$ transport in relation to mucus secretion from submucosal glands. *JOP.* 2:280–284.

Joo, N.S., J.V. Wu, M.E. Krouse, Y. Saenz, and J.J. Wine. 2001b. Optical method for quantifying rates of mucus secretion from single submucosal glands. *Am. J. Physiol. Lung Cell. Mol. Physiol.* 281:L458–L468.

Joo, N.S., T. Irokawa, J.V. Wu, R.C. Robbins, R.I. Whyte, and J.J. Wine. 2002a. Absent secretion to vasoactive intestinal peptide in cystic fibrosis airway glands. *J. Biol. Chem.* 277:50710–50715.

Joo, N.S., Y. Saenz, M.E. Krouse, and J.J. Wine. 2002b. Mucus secretion from single submucosal glands of pig. Stimulation by carbachol and vasoactive intestinal peptide. *J. Biol. Chem.* 277:28167–28175.

Joo, N.S., T. Irokawa, R.C. Robbins, and J.J. Wine. 2006. Hyposecretion, not hyperabsorption, is the basic defect of cystic fibrosis airway glands. *J. Biol. Chem.* 281:7392–7398.

Kang'ethe, W., K.G. Aimanova, A.K. Pullikuth, and S.S. Gill. 2007. NHE8 mediates amiloride-sensitive Na^+/H^+ exchange across mosquito Malpighian tubules and catalyzes Na^+ and K^+ transport in reconstituted proteoliposomes. *Am. J. Physiol. Renal Physiol.* 292:F1501–F1512.

Klanke, C.A., Y.R. Su, D.F. Callen, Z. Wang, P. Meneton, N. Baird, R.A. Kandasamy, J. Orlowski, B.E. Otterud, M. Leppert, et al. 1995. Molecular cloning and physical and genetic mapping of a novel human Na^+/H^+ exchanger (NHE5/SLC9A5) to chromosome 16q22.1. *Genomics.* 25:615–622.

Ko, S.B., W. Zeng, M.R. Dorwart, X. Luo, K.H. Kim, L. Millen, H. Goto, S. Naruse, A. Soyombo, P.J. Thomas, and S. Muallem. 2004. Gating of CFTR by the STAS domain of SLC26 transporters. *Nat. Cell Biol.* 6:343–350.

Lee, M.G., J.Y. Choi, X. Luo, E. Strickland, P.J. Thomas, and S. Muallem. 1999a. Cystic fibrosis transmembrane conductance regulator regulates luminal $Cl^-/HCO3^-$ exchange in mouse submandibular and pancreatic ducts. *J. Biol. Chem.* 274:14670–14677.

Lee, M.G., W.C. Wigley, W. Zeng, L.E. Noel, C.R. Marino, P.J. Thomas, and S. Muallem. 1999b. Regulation of Cl^-/ HCO_3^- exchange by cystic fibrosis transmembrane conductance regulator expressed in NIH 3T3 and HEK 293 cells. *J. Biol. Chem.* 274:3414–3421.

Lee, R.J., M.P. Limberis, M.F. Hennessy, J.M. Wilson, and J.K. Foskett. 2007. Optical imaging of Ca^{2+}-evoked fluid secretion by murine nasal submucosal gland serous acinar cells. *J. Physiol.* 582:1099–1124.

Lee, S.H., T. Kim, E.S. Park, S. Yang, D. Jeong, Y. Choi, and J. Rho. 2008. NHE10, a novel osteoclast-specific member of the Na^+/H^+ exchanger family, regulates osteoclast differentiation and survival. *Biochem. Biophys. Res. Commun.* 369:320–326.

Liu, J., Z. Diwu, and W.Y. Leung. 2001. Synthesis and photophysical properties of new fluorinated benzo[c]xanthene dyes as intracellular pH indicators. *Bioorg. Med. Chem. Lett.* 11:2903–2905.

Malo, M.E., and L. Fliegel. 2006. Physiological role and regulation of the Na^+/H^+ exchanger. *Can. J. Physiol. Pharmacol.* 84:1081–1095.

Manganel, M., and R.J. Turner. 1989. Agonist-induced activation of Na^+/H^+ exchange in rat parotid acinar cells. *J. Membr. Biol.* 111:191–198.

Manganel, M., and R.J. Turner. 1990. Agonist-induced activation of Na^+/H^+ exchange in rat parotid acinar cells is dependent on calcium but not on protein kinase C. *J. Biol. Chem.* 265:4284–4289.

Manganel, M., and R.J. Turner. 1991. Rapid secretagogue-induced activation of Na^+H^+ exchange in rat parotid acinar cells. Possible interrelationship between volume regulation and stimulus-secretion coupling. *J. Biol. Chem.* 266:10182–10188.

Masereel, B., L. Pochet, and D. Laeckmann. 2003. An overview of inhibitors of Na^+/H^+ exchanger. *Eur. J. Med. Chem.* 38:547–554.

Melvin, J.E., D. Yule, T. Shuttleworth, and T. Begenisich. 2005. Regulation of fluid and electrolyte secretion in salivary gland acinar cells. *Annu. Rev. Physiol.* 67:445–469.

Nakamura, N., S. Tanaka, Y. Teko, K. Mitsui, and H. Kanazawa. 2005. Four Na^+/H^+ exchanger isoforms are distributed to Golgi and post-Golgi compartments and are involved in organelle pH regulation. *J. Biol. Chem.* 280:1561–1572.

Nguyen, H.V., G.E. Shull, and J.E. Melvin. 2000. Muscarinic receptor-induced acidification in sublingual mucous acinar cells: loss of pH recovery in Na^+-H^+ exchanger-1 deficient mice. *J. Physiol.* 523(Pt 1):139–146.

Nguyen, H.V., A. Stuart-Tilley, S.L. Alper, and J.E. Melvin. 2004. $Cl^-/HCO(3)^-$ exchange is acetazolamide sensitive and activated by a muscarinic receptor-induced $[Ca^{2+}]_i$ increase in salivary acinar cells. *Am. J. Physiol. Gastrointest. Liver Physiol.* 286:G312–G320.

Okada, M., Y. Saito, E. Sawada, and A. Nishiyama. 1991. Microfluorimetric imaging study of the mechanism of activation of the Na^+/H^+ antiport by muscarinic agonist in rat mandibular acinar cells. *Pflugers Arch.* 419:338–348.

Orlowski, J., and S. Grinstein. 2004. Diversity of the mammalian sodium/proton exchanger SLC9 gene family. *Pflugers Arch.* 447:549–565.

Park, K., J.A. Olschowka, L.A. Richardson, C. Bookstein, E.B. Chang, and J.E. Melvin. 1999. Expression of multiple Na^+/H^+ exchanger isoforms in rat parotid acinar and ductal cells. *Am. J. Physiol.* 276:G470–G478.

Park, K., R.L. Evans, G.E. Watson, K. Nehrke, L. Richardson, S.M. Bell, P.J. Schultheis, A.R. Hand, G.E. Shull, and J.E. Melvin. 2001. Defective fluid secretion and NaCl absorption in the parotid glands of Na^+/H^+ exchanger-deficient mice. *J. Biol. Chem.* 276:27042–27050.

Park, M., S.B. Ko, J.Y. Choi, G. Muallem, P.J. Thomas, A. Pushkin, M.S. Lee, J.Y. Kim, M.G. Lee, S. Muallem, and I. Kurtz. 2002. The cystic fibrosis transmembrane conductance regulator interacts with and regulates the activity of the HCO_3^- salvage transporter human Na^+-HCO_3^- cotransport isoform 3. *J. Biol. Chem.* 277:50503–50509.

Parvin, M.N., T. Gerelsaikhan, and R.J. Turner. 2007. Regions in the cytosolic C-terminus of the secretory Na^+-K^+-$2Cl^-$ cotransporter NKCC1 are required for its homodimerization. *Biochemistry.* 46:9630–9637.

Poulsen, J.H., H. Fischer, B. Illek, and T.E. Machen. 1994. Bicarbonate conductance and pH regulatory capability of cystic fibrosis transmembrane conductance regulator. *Proc. Natl. Acad. Sci. USA.* 91:5340–5344.

Putney, L.K., S.P. Denker, and D.L. Barber. 2002. The changing face of the Na^+/H^+ exchanger, NHE1: structure, regulation, and cellular actions. *Annu. Rev. Pharmacol. Toxicol.* 42:527–552.

Qu, Z.H., and C. Hartzell. 2000. Anion permeation in Ca^{2+}-activated Cl^- channels. *J. Gen. Physiol.* 116:825–844.

Quinton, P.M. 1999. Physiological basis of cystic fibrosis: a historical perspective. *Physiol. Rev.* 79:S3–S22.

Quinton, P.M. 2001. The neglected ion: HCO_3. *Nat. Med.* 7:292–293.

Raphael, G.D., E.V. Jeney, J.N. Baraniuk, I. Kim, S.D. Meredith, and M.A. Kaliner. 1989. Pathophysiology of rhinitis. Lactoferrin and lysozyme in nasal secretions. *J. Clin. Invest.* 84:1528–1535.

Renner, E.L., J.R. Lake, M. Persico, and B.F. Scharschmidt. 1989. Na^+-H^+ exchange activity in rat hepatocytes: role in regulation of intracellular pH. *Am. J. Physiol.* 256:G44–G52.

Robertson, M.A., and J.K. Foskett. 1994. Na^+ transport pathways in secretory acinar cells: membrane cross talk mediated by $[Cl^-]i$. *Am. J. Physiol.* 267:C146–C156.

Robertson, M.A., M. Woodside, J.K. Foskett, J. Orlowski, and S. Grinstein. 1997. Muscarinic agonists induce phosphorylation-independent activation of the NHE-1 isoform of the Na^+/H^+ antiporter in salivary acinar cells. *J. Biol. Chem.* 272:287–294.

Roos, A., and W.F. Boron. 1981. Intracellular pH. *Physiol. Rev.* 61:296–434.

Salinas, D., P.M. Haggie, J.R. Thiagarajah, Y. Song, K. Rosbe, W.E. Finkbeiner, D.W. Nielson, and A.S. Verkman. 2005. Submucosal gland dysfunction as a primary defect in cystic fibrosis. *FASEB J.* 19:431–433.

Schwark, J.R., H.W. Jansen, H.J. Lang, W. Krick, G. Burckhardt, and M. Hropot. 1998. S3226, a novel inhibitor of Na^+/H^+ exchanger subtype 3 in various cell types. *Pflugers Arch.* 436:797–800.

Song, Y., and A.S. Verkman. 2001. Aquaporin-5 dependent fluid secretion in airway submucosal glands. *J. Biol. Chem.* 276:41288–41292.

Song, Y., D. Salinas, D.W. Nielson, and A.S. Verkman. 2006. Hyperacidity of secreted fluid from submucosal glands in early cystic fibrosis. *Am. J. Physiol. Cell Physiol.* 290:C741–C749.

Thiagarajah, J.R., Y. Song, P.M. Haggie, and A.S. Verkman. 2004. A small molecule CFTR inhibitor produces cystic fibrosis-like submucosal gland fluid secretions in normal airways. *FASEB J.* 18:875–877.

Thomas, R.C. 1984. Experimental displacement of intracellular pH and the mechanism of its subsequent recovery. *J. Physiol.* 354:3P–22P.

Trout, L., J.T. Gatzy, and S.T. Ballard. 1998a. Acetylcholine-induced liquid secretion by bronchial epithelium: role of Cl^- and HCO_3^- transport. *Am. J. Physiol.* 275:L1095–L1099.

Trout, L., M. King, W. Feng, S.K. Inglis, and S.T. Ballard. 1998b. Inhibition of airway liquid secretion and its effect on the physical properties of airway mucus. *Am. J. Physiol.* 274:L258–L263.

Trout, L., M.R. Corboz, and S.T. Ballard. 2001. Mechanism of substance P-induced liquid secretion across bronchial epithelium. *Am. J. Physiol. Lung Cell. Mol. Physiol.* 281:L639–L645.

Van Gelder, R.N., M.E. von Zastrow, A. Yool, W.C. Dement, J.D. Barchas, and J.H. Eberwine. 1990. Amplified RNA synthesized from limited quantities of heterogeneous cDNA. *Proc. Natl. Acad. Sci. USA.* 87:1663–1667.

Wang, D., S.M. King, T.A. Quill, L.K. Doolittle, and D.L. Garbers. 2003. A new sperm-specific Na^+/H^+ exchanger required for sperm motility and fertility. *Nat. Cell Biol.* 5:1117–1122.

Weintraub, W.H., and T.E. Machen. 1989. pH regulation in hepatoma cells: roles for Na-H exchange, Cl-HCO3 exchange, and Na-HCO3 cotransport. *Am. J. Physiol.* 257:G317–G327.

Wine, J.J., and N.S. Joo. 2004. Submucosal glands and airway defense. *Proc. Am. Thorac. Soc.* 1:47–53.

Wu, J.V., M. Krouse, and J.J. Wine. 2006. Acinar origin of Cftr-dependent airway submucosal gland fluid secretion. *Am. J. Physiol. Lung Cell Mol. Physiol.* 292:L304–L311.

Yang, C.M., J.M. Farley, and T.M. Dwyer. 1988. Muscarinic stimulation of submucosal glands in swine trachea. *J. Appl. Physiol.* 64:200–209.

Zachos, N.C., M. Tse, and M. Donowitz. 2005. Molecular physiology of intestinal Na^+/H^+ exchange. *Annu. Rev. Physiol.* 67:411–443.

Zhang, J., I.A. Bobulescu, S. Goyal, P.S. Aronson, M.G. Baum, and O.W. Moe. 2007. Characterization of Na^+/H^+ exchanger NHE8 in cultured renal epithelial cells. *Am. J. Physiol. Renal Physiol.* 293:F761–F766.